Making hypervelocity stars

Frans Forsberg

Lund Observatory
Lund University

2020-EXA163

Degree project of 15 higher education credits
June 2020

Supervisor: Melvyn B. Davies

Lund Observatory
Box 43
SE-221 00 Lund
Sweden

Abstract

In this thesis, I investigate if the binaries that are being tidally disrupted by means of the Hills mechanism, producing hypervelocity stars, could have been transported to the galactic centre by two-body scattering. To survive a scattering event, the binary must be hard, meaning that the binding energy of the binary is higher than the kinetic energy of the collider. If the binary is soft, the binary is disrupted at the scattering event and cannot contribute to the production of hypervelocity stars. From 43 observed hypervelocity stars, I calculate a distribution of the binary separation for each binary prior to disruption. Assuming that the mass of the collider is 1 $M_{\odot}$, the fraction of binaries considered hard in the distribution is calculated for three binary mass ratios, 2:1, 1:1, 1:2, between the ejected and captured star and distances from the galactic centre, 0.1, 0.3, 1 pc. No binaries within 0.1 pc could be considered hard since the limiting binary separation at that distance from the galactic centre is less than the physical size of both binary components. For binaries with a mass ratio of 1:2, scattered 1 pc from the galactic centre, $10^{-2} - 10^{-1}$ of all binaries would be considered hard. Equivalently, to sustain the expected disruption rate of 10^{-5} yr^{-1}, 100-1000 binaries needs to two-body scatter every 1 Myr. The observations of B-stars on highly eccentric orbits around Sgr A*, so called S-stars, indicate that hypervelocity stars might be produced by higher mass binaries, corresponding to a mass ratio of 1:4 for the observed hyper velocity stars. This increase in mass increases the fraction of hard binaries by magnitude of 10. This is still too inefficient to solely sustain the expected disruption rate without depleting the galactic centre of stars within 1 pc. Although, the possibility of a 1:4 mass ratio S-star binary surviving a scattering event is large enough to not rule out as possible origin of individual hypervelocity stars.

Populärvetenskaplig beskrivning

Hypervelocity stars, på svenska hyperhastighetsstjärnor, är stjärnor som observerats med så hög hastighet att de kan lämna vår galax, Vintergatan. Den första hyperhastighetsstjärnan upptäcktes av R. Brown m. fl. (2005), och sedan dess har många fler upptäckts. J. G. Hills presenterade (1988) en teori om att hyperhastighetsstjärnor härstammar från binära stjärnor (två stjärnor som kretsar varandra) som interagerar med det supermassiva svarta hålet i Vintergatans centrum. Ett fenomen kallat *Hills Mekanismen*, se Figur 3.1.

När den binära stjärnan kommer för nära det svarta hålet, slits den isär av det enorma gravitationsfältet. En av stjärnorna fångas i omloppsbana runt det svarta hålet medans den andra stjärnan slungas iväg ut i rymden. Föreställ dig två tennisbollar sammankopplade med en tråd. Om du snurrar tennisbollarna så fort du kan och plötsligt klipper av tråden, då flyger tennisbollen du inte höll i handen iväg med hög hastighet.

För att en sådan splittring ska kunna ske, måste den binära stjärnan komma väldigt nära det svarta hålet, betydligt närmare än vad som tidigare observerats. Detta innebär att det måste existera någon process som styr de binära stjärnorna mot galaxens centrum, t.ex. kollisioner eller andra massiva objekt som kan ändra på den binära stjärnans riktning. Målet med min avhandling är att undersöka olika transportmetoder. Varje transportmetod kommer fodra specifika egenskaper hos den binära stjärnan, t.ex. massa eller hastighet. Från de observerade hyperhastighetsstjärnorna kan egenskaperna hos den tillhörande binära stjärnan beräknas med hjälp av teorin föreslagen av J. G. Hills. Egenskaperna av den beräknade binära stjärnan kan sedan jämföras med de begärda egenskaperna av varje transportmetod.

Galaxens centrum är ett av de svåraste områdena att observera p.g.a. allt ljus från den stora stjärnpopulationen och även stora mängder damm. Försök urskilja en tänd tändsticka framför en strålkastare, i en sandstorm. När J. G. Hills föreslog sin teori om hyperhastighetsstjärnor för andra astronomer var det för att bevisa existensen av ett supermassivt svart hål i galaxens centrum. Idag är existensen av Vintergatans svarta hål Sgr A* bekräftad, men hyperhastighetsstjärnor kan fortfarande vara till stor hjälp för oss genom att få en bättre uppfattning om klimatet för himlakroppar i galaxens centrum. Alla framsteg inom dynamiken av galaxens centrum kan vara viktiga för åtskilliga inriktningar inom astronomi.

Contents

List of Figures

List of Tables

Chapter 1

Introduction

Hypervelocity stars (HVS) are stars that have been observed at speeds high enough to escape the Milky Way. The first HVS was observed by Brown et al. (2005), where a B-type star was discovered far out in the galactic halo, moving with a speed of over twice the galactic escape speed. HVS have been shown to have galactic centre origin by e.g. Svensson et al. (2008) and Brown et al. (2018). Hills (1988) predicted the existence of HVS as a consequence of binary stars being tidally disrupted when having close encounters with a *super massive black hole* (SMBH), called the Hills mechanism. When the binary is disrupted, the star closest to the SMBH is captured in a highly eccentric orbit and the other star is ejected at speeds of up to 4000 km s^{-1}, according to simulations preformed by Hills (1988). The observed S-stars in orbits around Sgr A*, are thought to be these captured stars (by e.g. Generozov and Madigan (2020)). Through numerical simulations and the theory by Hills (1988), Bromley et al. (2006) derived equations describing how the probability of ejection, and the velocity of the ejected HVS, depends on the binary separation, mass of the binary components, and distance to the SMBH at disruption.

For binary disruption to occur through the Hills mechanism, a binary must be within $\sim$100 AU from the SMBH. To this day, no binaries have ever been observed within that range from Sgr A*. Hence, there must be some process that transports these binaries towards the galactic centre if the observed HVS are indeed produced by the Hills mechanism. Two-body scattering is a mechanism where two objects have a close encounter in space and exchange kinetic energy and momentum through gravity. Since a binary star cannot be considered a rigid body, the binary will be disrupted at the scattering event if the kinetic energy of the collider is higher than the binding energy of the binary. If a binary is disrupted at the scattering event, it cannot contribute to the production of HVS.

I will in this thesis calculate the properties of the original binaries from 43 observed HVS, taken from Brown et al. (2014) and Bromley et al. (2018), using a model of the galactic potential by Paczynski (1990) and the equations derived by Bromley et al. (2006). From the properties of the original binaries, I will investigate the possibility of binaries being sent on black hole encountering orbits by means of two-body scattering, and compare

the result with predictions of other transportation methods.

Chapter 2

Observations of Hypervelocity Stars

The first detection of an HVS was confirmed by Brown et al. (2005) when the unbound star 'SDSS J090745.0+024507' was detected with *Sloan Digital Sky Survey* photometry and observed with the 6.5 m *Multiple Mirror Telescope* (MMT). The galactic halo consists of mainly old, red, low mass stars, but also low mass *blue horizontal branch* (BHB) stars. Their purpose was to measure the velocity of these BHB stars. By adding red and blue filters to the photometry they could distinguish the blue stars from the red, and then target the stars with spectroscopy to determine their radial velocity. What they discovered was a blue MS star far up in the halo moving at twice the galactic escape speed, previously never observed in the halo.

This discovery motivated a thorough targeted HVS survey with the MMT telescope. As of today, MMT has found 42 HVS in the galactic halo with radial velocities exceeding +275 km s^{-1}, Kreuzer et al. (2020). The latest addition to the catalogue of observed HVS comes from the Gaia DR2 release, which can detect high speed stars closer to the galactic plane because of its high precision 6D phase-space measurement. The Gaia telescope measures three positional coordinates; right ascension (α), declination (δ), and parallax (ω), and three velocities; proper motion (μ_α, μ_δ), and radial velocity (**RV**). Svensson et al. (2008) stated that observed HVS are mainly blue MS stars and have origin in the galactic centre based on their unbound trajectories. Yet, there have been instances where HVS have originated from other places, such as Gualandris and Portegies Zwart (2007) suggesting that the HVS HE 0437-5439 originated from the *Large Magellanic Cloud*.

In this thesis, I will focus on the two largest collections of hypervelocity stars. My HVS catalogue consists of 43 stars, 18 of them discovered by the MMT survey, taken from Brown et al. (2014), and 25 of them discovered by Gaia, taken from Bromley et al. (2018). All stars are listed in Table A.1 & A.2. I choose this set of stars based on the apparent differences. The MMT stars are positioned much further out in the galaxy compared to the Gaia stars, ranging from 49-113 kpc from the galactic centre whilst the Gaia stars are located at distances ranging from 4-15 kpc. Since the MMT stars are much further away from our solar system, radial velocity measurements yield a much higher precision in

galactic rest frame velocity, v_g, compared to the Gaia stars located closer to the galactic plane. However, since the Gaia stars are closer, positional measurements are more accurate. This allows for a broad representation of observed HVS.

Chapter 3

How to produce Hypervelocity Stars: The Hills Mechanism

The observed HVS have origin in the galactic centre. The observed velocity of the HVS can only be explained by an interaction with a massive compact object. Hills (1988) predicted the existence of HVS, caused by binary stars having close encounters with a SMBH in the centre of the Milky Way, called the Hills Mechanism. The enormous gravitational field of the SMBH disrupts the binary, capturing one of the binary components, and ejecting the other star at high speeds, see Figure 3.1. Within ~ 0.01 pc from the SMBH, an isotropic cluster of young B-stars have been observed, called S-stars. These S-stars are theorised to be the captured stars of tidally disrupted binaries, whose observed thermal eccentricity is then relaxed by some additional process (e.g. Generozov and Madigan (2020)). If the binary approaches the black hole at escape speed on a parabolic trajectory, the velocity of the binary's centre of mass is then

$$v_{cm} = \sqrt{\frac{2GM_{bh}}{R}}, \tag{3.1}$$

where R is the distance from the binary to the SMBH and M_{bh} is the mass of the SMBH. Notice the factor 2 in the nominator as for parabolic encounters. The orbital velocity of the stars within the binary is

$$v = \sqrt{\frac{G(m_1 + m_2)}{a_{bin}}}, \tag{3.2}$$

where m_1 and m_2 is the mass of the binary components and a_{bin} is the binary separation. The binary is tidally disrupted by the tidal field of the SMBH when the binary is within the tidal splitting radius, R_{min}.

$$R_{min} \simeq a_{bin} \left(\frac{M_{bh}}{m_1 + m_2} \right)^{1/3} \tag{3.3}$$

where M_{bh} is the mass of the black hole. The tidal splitting radius is usually of order 100 AU, whilst the binary separation is of order 1 AU. The mass of the SMBH in the Milky

Way, Sgr A*, is of order 10^6 $M_\odot$, meaning that we can expect v_{cm} to be approximately 100 times larger than v.

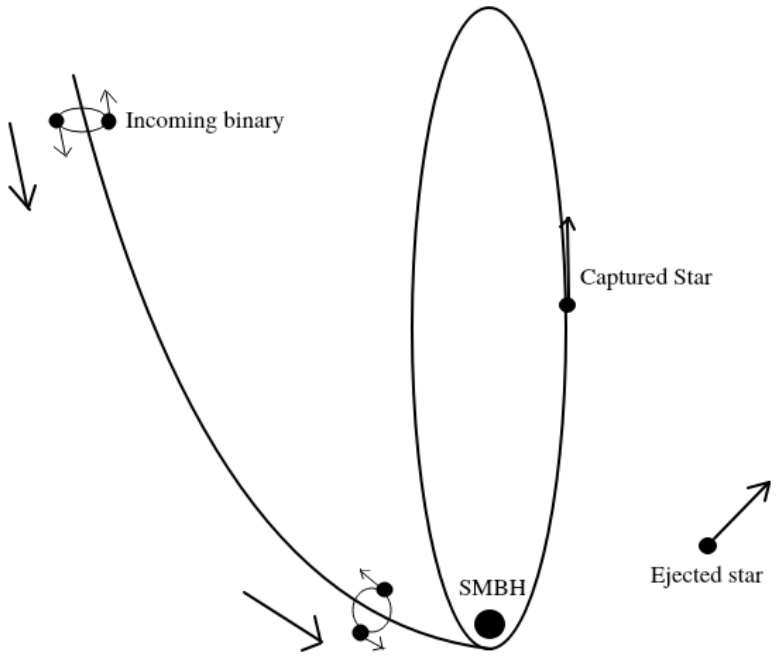

Figure 3.1: Illustration of a binary being tidally disrupted via the Hills mechanism.

When the binary is tidally disrupted, one star is captured in a highly eccentric orbit around the SMBH, and the other star is ejected at a high speed. The ejected star gains the excess energy from the captured star, allowing it to reach speed of up to 1400 km s^{-1} for an equal mass, 2 $M_\odot$ binary with $a_{bin} = 0.1$ AU (Hills (1988)). Bromley et al. (2006) derived an expression for calculating the ejection speed using numerical simulations, assuming that the initial approach speed of the binary at infinity is 250 km s^{-1} and that the orbits of the binary components are circular ($e = 0$).

$$v_{ej} = 1760 \left(\frac{a_{bin}}{0.1\ \text{AU}}\right)^{-1/2} \left(\frac{m_1 + m_2}{2\ M_\odot}\right)^{1/3} \left(\frac{M_{bh}}{3.5 \cdot 10^6\ M_\odot}\right)^{1/6} f_r\ \text{km s}^{-1}, \tag{3.4}$$

were a_{bin} is the binary separation, m_1 and m_2 are the masses of the ejected and captured star, and M_{bh} is the black hole mass. The factor f_r is a tuning factor of order unity used to match ejection velocity with numerical simulations. The tuning factor takes the shape of a fifth degree polynomial (see Figure 3.2),

$$f_r = 0.774 + 0.0204D - 6.23 \cdot 10^{-4} D^2 + 7.62 \cdot 10^{-6} D^3 - 4.24 \cdot 10^{-8} D^4 + 8.62 \cdot 10^{-11} D^5, \tag{3.5}$$

where D is dimensionless parameter called the Hills parameter.

$$D = \left(\frac{R_{min}}{a_{bin}}\right) \left[\frac{2M_{bh}}{10^6(m_1 + m_2)}\right]^{-1/3} \tag{3.6}$$

From numerical simulations of v_{ej} and physical constraints on the binary separation, based on the radius of the binary components and ejection speeds high enough to populate the galaxy beyond 10 kpc, Bromley et al. (2006) concluded that the Hills parameter can take on the values $0 \leq D \leq 175$. From that range, they derived an expression for the probability of an interaction leading to an ejection of a star.

$$P_{ej} \approx 1 - \frac{D}{175} \tag{3.7}$$

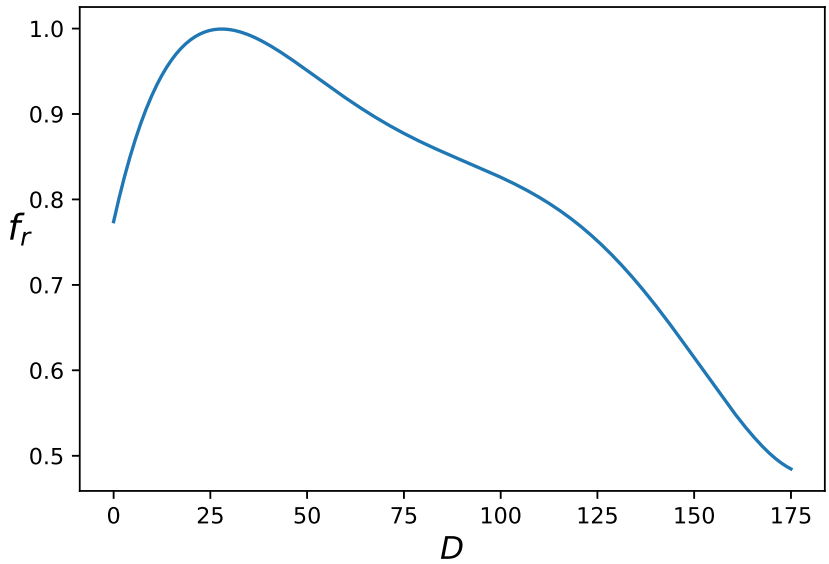

Figure 3.2: The fifth degree fitting polynomial, f_r, plotted as a function of the Hills parameter, D, in the range possible to produce an ejected HVS. Notice how the range of f_r spans a factor of 2.

According to the simulations performed by Bromley et al. (2006), the star closer to the SMBH at the moment of disruption is captured. However, Sari et al. (2010) showed that both stars have an equal probability of being captured for reasonable mass ratios, $q = m_1/m_2$. Only for binaries with extreme mass ratio ($q < 1/10$) are the more massive stars more likely to be ejected. Because lighter stars move more from the binaries centre of mass, it faces a higher risk of being captured. It should be noted that these cases do not result in as great ejection speeds. For unequal mass binaries, the ejection speed of the primary and secondary is

$$v_1 = v_{ej}\left(\frac{2m_2}{m_1+m_2}\right)^{1/2}, \quad v_2 = v_{ej}\left(\frac{2m_1}{m_1+m_2}\right)^{1/2}, \tag{3.8}$$

respectively. The energy released at disruption if the same no matter which star is ejected, but the velocity of the ejected star is limited by its mass.

Chapter 4

Calculating Initial Conditions

Knowing that the observed HVS in my catalogue most likely have origin in the galactic centre, I seek the properties of the original binaries prior to being tidally disrupted through the Hills Mechanism. First and foremost, the observed position of the HVS with respect to the galactic centre must be determined.

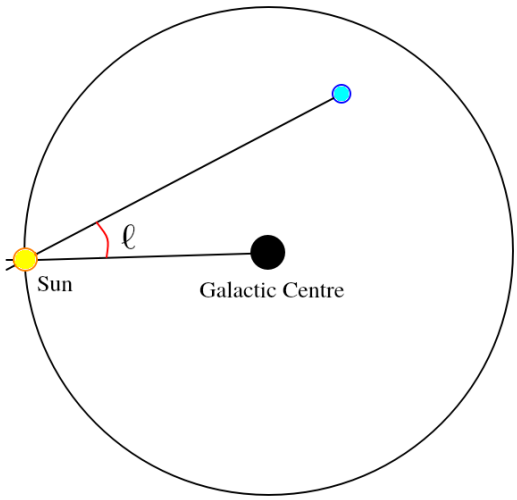

(a) Galactic plane face on.

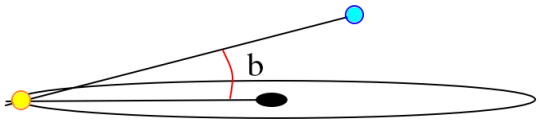

(b) Galactic plane edge on.

Figure 4.1: Illustration of galactic coordinates (ℓ, b), where ℓ and b is the galactic longitude and latitude, respectively. The coordinate system is right-hand oriented, meaning that the positive direction is east and north with respect to the fundamental plane.

In Bromley et al. (2018), I am given the parallax, ω, galactocentric distance, R_g, and the galactic coordinates (ℓ, b) for all Gaia stars, from which I calculate the galctocentric cylindrical coordinates, (R, z). Galctocentric cylindrical coordinates means that R is the radial distance from the galactic centre and z is the distance from the galactic plane. For the measured parallax, all relative errors $\sigma_\omega/\omega < 0.2$, which corresponds to a 5σ detection. When the relative error distribution is much smaller than the parallax itself,

the tails extending to infinity of the Gaussian distribution become negligible and thus the heliocentric distance can be calculated using the inverse law $d_h = 1/\omega$, without producing unrealistic distances for a star in the Milky Way. A more general approach would be Bayesian inference, which incorporates prior information about the objects location. It will be noticeable in Chapter 5 that the results are in fact not very sensitive to changes in the star's position, hence why I opted for this simpler approach.

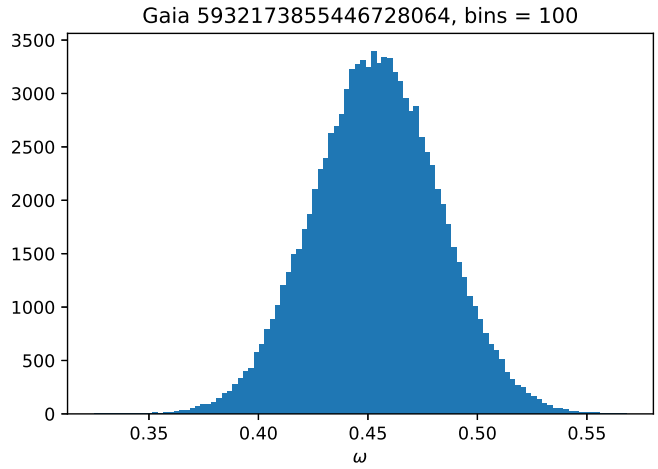

Figure 4.2: Gaussian distribution of the observed parallax of Gaia '5932173855446728064' for a 5σ detection.

With the calculated heliocentric distance, and given R_g, (R, z) can simply be calculated since

$$z = d_h \sin b \tag{4.1}$$

and

$$R = \sqrt{R_g^2 - z^2}, \tag{4.2}$$

see Figure 4.1.

When calculating the position of the stars in the MMT sample, I need to take a different approach since I am not given the measured parallax in either Brown et al. (2014) or previous records of the included stars (e.g. Brown et al. (2012)). What I am given is R_g and (ℓ, b). By describing the vector from our solar system to the star as

$$\underline{r} = \lambda \begin{pmatrix} 1 \\ \alpha \\ \beta \end{pmatrix} \Longrightarrow \begin{cases} x = \lambda \\ y = \lambda\alpha \\ z = \lambda\beta \end{cases} \tag{4.3}$$

where

$$\alpha = \tan(\ell), \quad \beta = \sqrt{1+\alpha^2}\tan(b), \tag{4.4}$$

and placing our solar system in the origin and the galactic centre in (8,0,0). This means that for some unique λ, $\underline{r} = (x, y, z)$ represents the position of the star and R_g can be described as

$$R_g = \sqrt{(\lambda - 8)^2 + (\lambda\alpha)^2 + (\lambda\beta)^2} \tag{4.5}$$

Knowing that the MMT stars are much further away from both the galactic centre and our solar system than the Gaia stars, the difference between d_h and R_g becomes less significant. Hence, I produce a Gaussian distribution of R_g using the reported σ for the width of the Gaussian. For each possible R_g in the distribution, there exist a unique λ for which equation (4.5) equals the expected value of R_g. The desired λ is found through rewriting the linear interpolation equation

$$\lambda = \lambda_A + (\lambda_B - \lambda_A)\frac{(R_{g,exp} - R_A)}{(R_B - R_A)}, \tag{4.6}$$

where $R_{g,exp}$ is the known galactocentric distance and the points A and B represents distances slightly shorter and longer than the expected distance, respectively. With λ calculated, z can be calculated through equation (4.3), and R through

$$R = \sqrt{(\lambda - 8)^2 + (\lambda\alpha)^2} \tag{4.7}$$

All calculated values for both Gaia and MMT stars are tabulated in Appendix B. For the Gaia stars, each distribution of ω will result in a distribution of possible positions for each Gaia star (Figure 4.3a). Equivalently, each distribution of R_g results in a distribution of possible positions for each MMT star (Figure 4.3b). This distribution of positions corresponds to multiple representations of the same star.

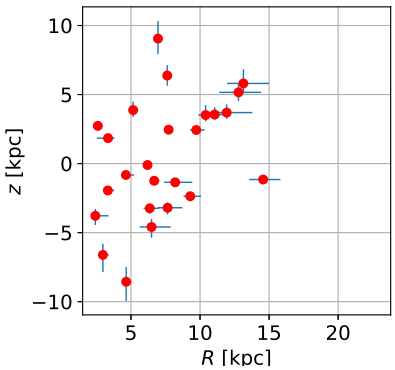

(a) Spatial distribution of Gaia stars.

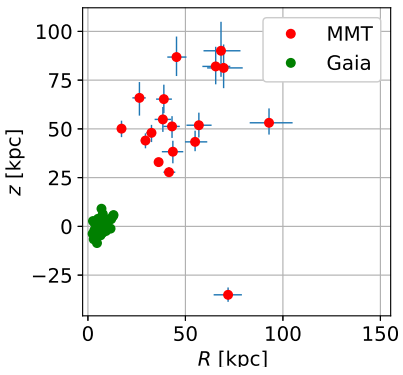

(b) Spatial distribution of MMT stars with the position of Gaia stars as reference.

Figure 4.3: Spatial distribution of both star samples. The error bars represents the full possible range in (R, z). The Gaia stars with seemingly no error bars are the stars closest to our solar system.

Chapter 5

Calculating Ejection Velocity

With the position of each HVS determined, the next step is to determine the ejection speed of each HVS. This can be done simply using the law of energy conservation:

$$\frac{1}{2}v_{ej}^2 + \Phi_0 = \frac{1}{2}v_g^2 + \Phi_1 \tag{5.1}$$

were v_{ej} is the ejection speed and v_g is the observed galactic rest frame velocity, and $\Phi_{0,1}$ is the galactic potential at the point of ejection and observation, respectively. Since the mass distribution of the galaxy is neither spherical or uniform, a more detailed model of the galactic potential that considers the change in density is needed. I use the model suggested by Paczynski (1990) which consists of three components. The first two components were proposed by Miyamoto and Nagai (1975) and describe the potential of the bulge and disk:

$$\Phi_B(R,z) = -\frac{GM_1}{(R^2 + [a_1 + (z^2 + b_1^2)^{1/2}]^2)^{1/2}}, \;\; R^2 = x^2 + y^2, \tag{5.2}$$

$$\Phi_D(R,z) = -\frac{GM_2}{(R^2 + [a_2 + (z^2 + b_2^2)^{1/2}]^2)^{1/2}}, \;\; R^2 = x^2 + y^2, \tag{5.3}$$

where Φ_B and Φ_D corresponds to the gravitational potential of the bulge and disk, respectively, and R and z are the galactocentric cylindrical coordinates. The bulge and disk components takes the shape of an ellipsoid, described by the parameters a and b. The third component that describes the halo potential, derived from the halo's central density, ρ_c, is of the form:

$$\Phi_H(R,z) = \frac{GM_c}{r_c}\left[\frac{1}{2}\ln\left(1 + \frac{r^2}{r_c^2}\right) + \frac{r_c}{r}\arctan\left(\frac{r}{r_c}\right)\right], \;\; r^2 = x^2 + y^2 + z^2. \tag{5.4}$$

where r_c is the halo core radius and $M_c \equiv 4\pi\rho_c r_c^3$. The complete model of the galactic potential is then the sum of all components, $\Phi = \Phi_B + \Phi_D + \Phi_H$, and all parameters used are summarised in Table 5.1.

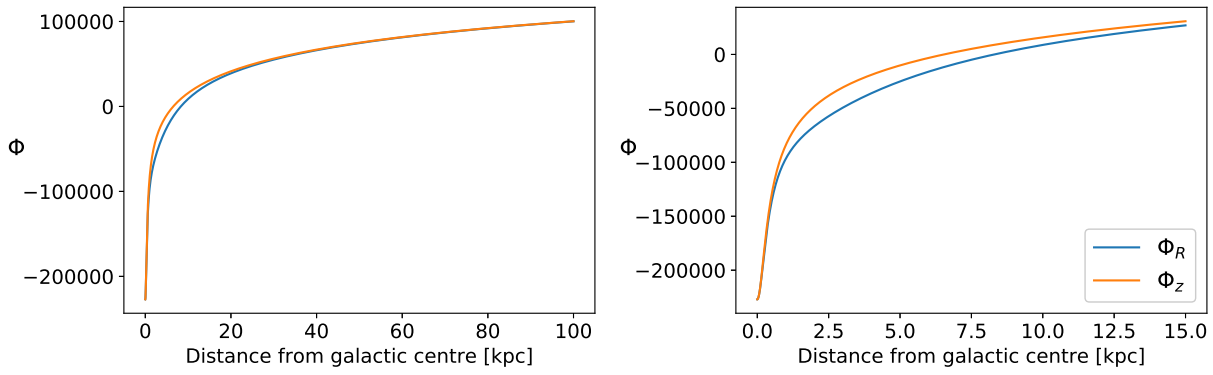

(a) (b)

Figure 5.1: (a) The model of the galactic potential plotted as a function of the distance from the galactic centre, both in the galactic plane and axially along z. (b) Closer view of the galactic potential to highlight the difference in action for both directions.

Table 5.1: We choose the same set of parameters for the potential as Paczynski (1990).

Parameters	Paczynski (1990)		
Φ_1	$a_1 = 0$ kpc	$b_1 = 0.277$ kpc	$M_1 = 1.12 \cdot 10^{10} M_\odot$
Φ_2	$a_2 = 3.7$ kpc	$b_2 = 0.20$ kpc	$M_2 = 8.07 \cdot 10^{10} M_\odot$
Φ_3	$r_c = 6.0$ kpc		$M_c = 5.0 \cdot 10^{10} M_\odot$

As seen in Figure 5.1, the galactic potential is close to, but not completely spherically symmetric. This difference arises because of the geometry of the potential components. The halo component is spherically symmetric, whereas the bulge and disk components are not. The disk component is of course the least spherical component of the two since it is more flattened. The difference in geometry can be shown by solving the Poisson's equation

$$\nabla^2 \Phi_i = 4\pi G \rho_i \tag{5.5}$$

and determine the density distribution, ρ_i, for each component.

With this model of the galactic potential I can calculate a distribution of v_{ej} from the distribution of possible initial positions. For the Gaia stars, I produce a Gaussian distribution of the observed v_g, where the error is 1σ. For each entry in the distribution of the initial position, I pick a random entry in the distribution of v_g, using `random.py`, and calculate the ejection speed v_{ej} using equation (5.1). For the MMT stars I use the central value given in Brown et al. (2014) for all possible positions. Since only the radial velocity of the MMT stars have been measured, their total velocity cannot be determined without the tangential component, and hence why no uncertainty in v_g can be made. All that is known from the radial velocity is at what rate the stars move relative to our solar system.

Luckily, since the MMT stars are so far away from both our solar system and the galactic centre, the difference between v_g and **RV** becomes less significant.

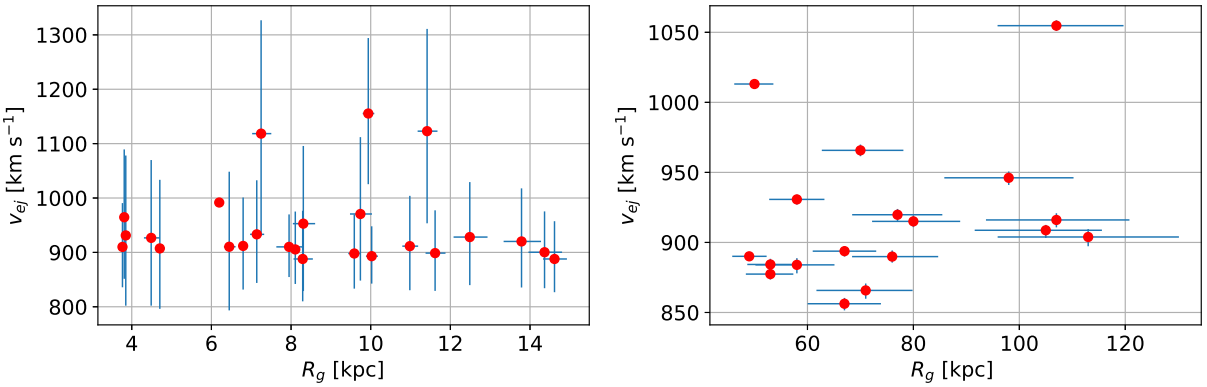

(a) Gaia DR2

(b) MMT

Figure 5.2: The distribution of ejection velocity and galactocentric distance for both star samples. The error bars represent 1σ uncertainty in ejection velocity and galactocentric distance.

In Figure 5.2 we see that the ejection velocity of the MMT stars calculated from the central value of v_g is very insensitive to changes in the distance from the galactic centre. This is reasonable since variations in position outside of the first kpc from the galactic centre corresponds to a small change in galactic potential compared to closer to the galactic centre (see Figure 5.1b). All stars are located outside of where the potential decreases most rapidly. Hence, the range in v_{ej} for Gaia stars arises almost solely from the observed range in v_g. According to this model of the potential, the escape speed of the galaxy when ejected at galactic centre is ∼810 km/s. Brown et al. (2018) states that HVS with ∼100km/s above escape speed has origin in the galactic centre. From the calculated v_{ej} in Appendix B we see that most stars have ejection velocities of $\sim$ 900 km s^{-1} or above, reconfirming their galactic centre origin.

Chapter 6

Calculating Binary Separation

In this section, I am going to calculate the binary separation of each original binary using the equations derived by Bromley et al. (2006) in Chapter 3. I start with rewriting equation (3.4), so that it can be solved for the binary separation:

$$a_{bin} = 0.1\left(\frac{1760}{v_{ej}}\left(\frac{m_1+m_2}{2M_\odot}\right)^{1/3}\left(\frac{M_{bh}}{3.5\cdot 10^6 M_\odot}\right)^{1/6} f_r\right)^2 \tag{6.1}$$

Next, the mass of Sgr A* is taken as $4\cdot 10^6 M_\odot$. For the MMT stars, I produce a Gaussian distribution of their mass, where the error is 1σ, given in Brown et al. (2014). For each calculated v_{ej}, I choose a random entry from the Gaussian distribution of masses. The mass of the Gaia stars are unknown since they all have evolved of the MS (see Figure 1 in Bromley et al. (2018)). The age of each star is needed to account for the stellar evolution so that the mass can be determined from their colour and apparent magnitude. Instead, I estimate the mass from the information given in Figure 6.1. The progression of v_{ej} for both samples is near identical, and the mass of the MMT stars ranges from 2-5 $M_\odot$. I decide to treat all Gaia stars as 3 $M_\odot$ stars. What also can be seen in Figure 6.1a, is that v_{ej} for the MMT stars is consistently trailing behind the v_{ej} of the Gaia stars. This is in agreement with the observed velocity of the MMT stars missing the tangential component.

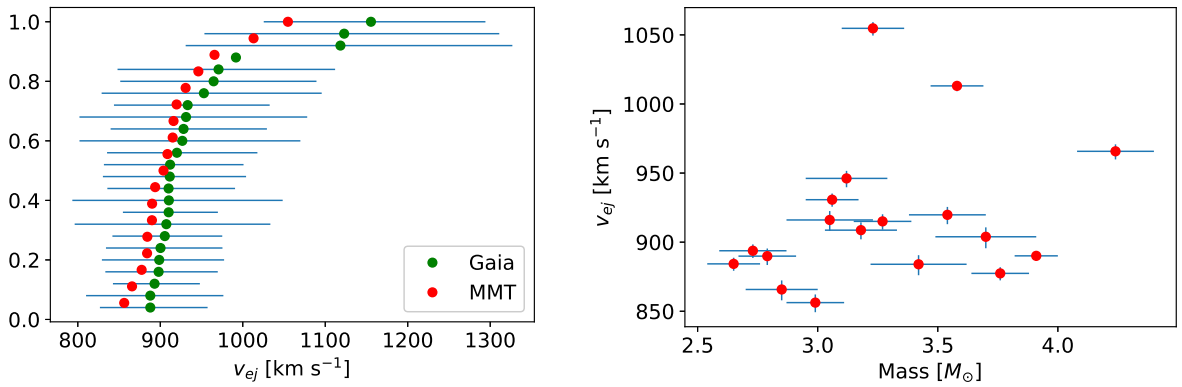

(a) (b)

Figure 6.1: (a) Cumulative plot of the ejection velocity comparing the progression for both star samples. The error bars represents 1σ uncertainty in v_{ej} for the Gaia stars. (b) Plot of the ejection velocity versus the range in mass for the MMT sample. The error bars represents 1σ uncertainty in mass and v_{ej}.

Since I assume that the HVS in my catalogue have been ejected, and that the probability of an encounter leading to an ejection depends on the Hills parameter, D, I do a Monte Carlo sampling of a large number of D's, uniformly distributed in the possible range $0 \leq D \leq 175$. If the probability, P, for a specific D is larger than some randomly generated number between (0,1), that value of D is kept. For this probabilistically separated distribution of D, a distribution of the fitting function, f_r, can be made (see Figure 6.2).

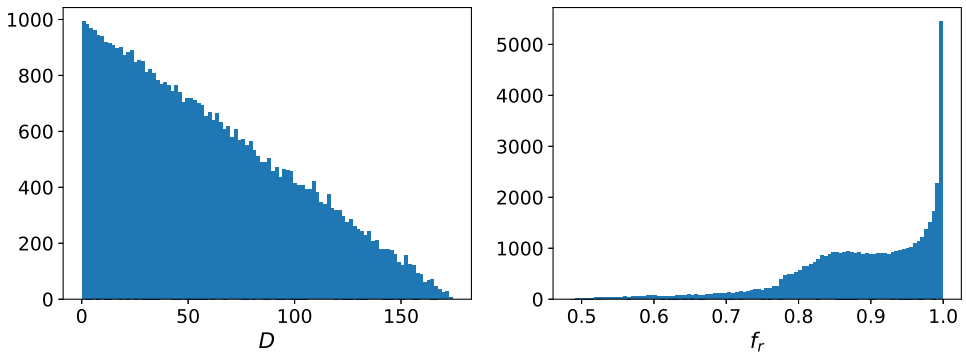

Figure 6.2: Acquired distribution of the Hills parameter, D, and fitting function, f_r, after Monte Carlo sampling. Each histogram has 100 bins.

To summarise, for each entry in the distribution of (R, z), corresponding to multiple representations of the same star, I choose a random value from the distribution of v_g for the Gaia stars, and the central value of v_g for the MMT stars, to calculate a distribution of v_{ej}. Then, for each entry in the distribution of v_{ej}, I choose random value from the distribution of mass values for the MMT stars, and the fixed estimated value of the mass

for the Gaia stars. Lastly, by choosing a final random value from the distribution of f_r, I can calculate the distribution of binary separation, a_{bin}, for all of the stars. This distribution of binary separation is calculated for each star, at three different mass ratios, 2:1, 1:1, and 1:2, between the ejected and captured star. Note, following the physical constraint proposed by Bromley et al. (2006), all binary separations smaller than 0.05 AU are discarded because of the physical size of the stars. Both stars needs to fit within the binary. A binary separation of 0.05 AU is approximately 10 $R_\odot$, equivalent to roughly twice the radius of a 4 $M_\odot$ star.

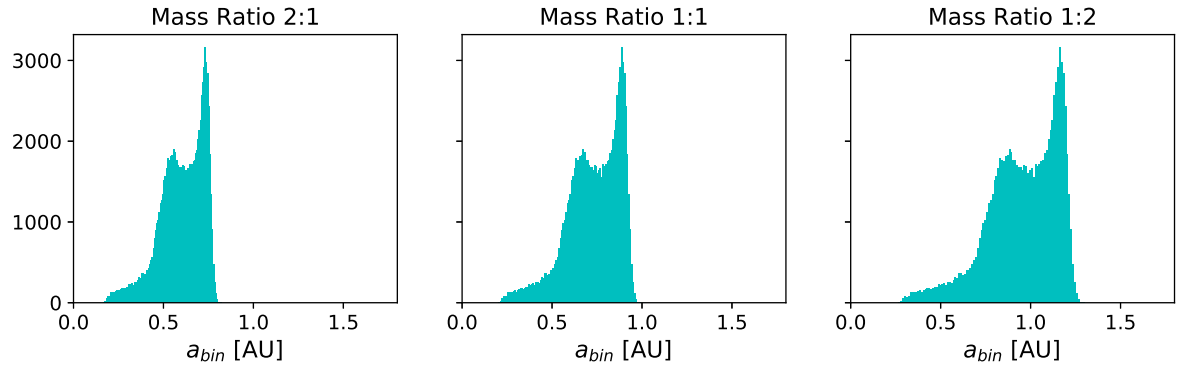

Figure 6.3: Distribution of a_{bin} for different mass ratios of the MMT star 'HVS 4'.

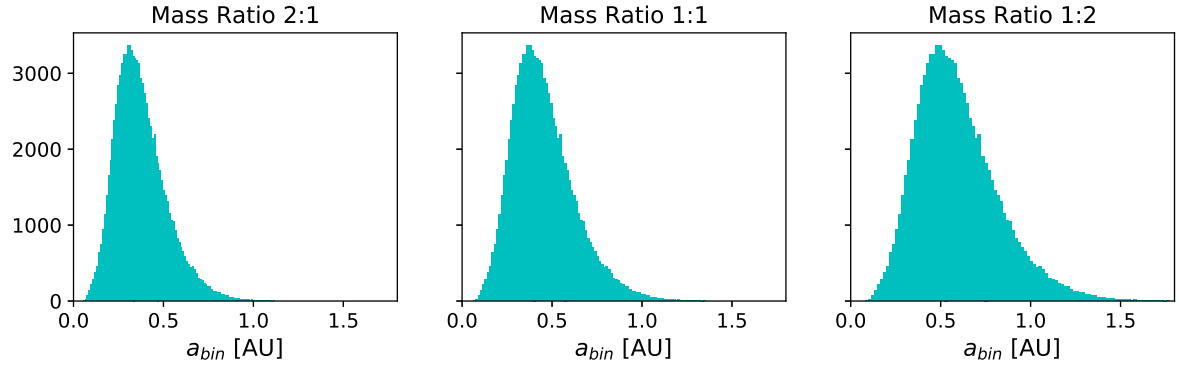

Figure 6.4: Distribution of a_{bin} for different mass ratios of the Gaia star '1478837543019912064'.

In Figure 6.3 we see that the a_{bin} distribution of the MMT star 'HVS 4' takes a shape reminiscent of the fitting function, f_r. However, in Figure 6.4 we see that the Gaia star '1478837543019912064' takes a more Gaussian shape. The range in v_{ej} for the Gaia stars is enough to dominate the shape of the a_{bin} distribution. On the contrary, the range in mass for the MMT stars are not the sole major contributor to the shape of the a_{bin} distribution.

Chapter 7

Transportation Method

Now that the properties of the original binaries are known, the remaining question is: Which process is most likely to send these binaries on black hole encountering orbits from outside of the tidal splitting radius, R_{min}? We know that it must be some process that feeds these binaries towards the galactic centre since no binary population has ever been observed close enough to Sgr A* to allow for star ejection via the Hills Mechanism. In this section, I will present plausible transportation methods, and if there are any, inferred constraints on the process.

7.1 Two-Body Scattering

The most intuitive answer to astronomical objects occasionally changing their direction of motion is random two-body scattering. This mechanism is built on the premise that two objects have a close encounter in space and exchanges kinetic energy and momentum by gravitationally deflecting each other. In this case our binaries and some other massive object. When the binary is on a circular orbit at some distance R_0 from the galactic centre, its velocity can be described as

$$v_{bin} = \sqrt{\frac{GM_{bh}}{R_0}} \tag{7.1}$$

I do not consider distances $R > 1$ pc, since at distances further out from the galactic centre, the enclosed mass of the stars within that distance is greater than the mass of the SMBH, meaning that M_{bh} cannot be assumed to dominate the gravitational potential (non-Keplerian) and equation (7.1) is no longer valid. Collisions can still occur outside of 1 pc, although a successful scattering is increasingly difficult for longer distances. If the colliding mass is assumed to have the same orbital speed as the binary with random direction of motion in the galactic plane. If the collision is head on, the relative velocity would be $2v_{bin}$, and if the objects were moving in parallel, the relative velocity would trivially zero. This means that on average, the velocity of each object is perpendicular to

each other, and the relative velocity is then

$$v_{rel} = \sqrt{v_{bin}^2 + v_3^2} = \sqrt{2} v_{bin}, \tag{7.2}$$

where v_3 is the velocity is the velocity of the colliding object.

Since a binary cannot be considered a rigid body, each binary faces a risk of being disrupted at the scattering event. To survive a scattering event, the binary must be *hard*. I consider a binary to be hard if its binding energy is higher than the kinetic energy of the collider

$$\frac{G m_1 m_2}{2 a_{bin}} \geq \frac{1}{2} m_3 v_{rel}^2, \tag{7.3}$$

where m_3 is the mass of the collider. This means that there exist a maximum binary separation, a_{max}, which allows a binary to be hard at given distance from the galactic centre and for given masses of the collider and binary components.

$$a_{max} = \frac{R_0}{2} \frac{m_1 m_2}{m_3 M_{bh}} \tag{7.4}$$

For all $a_{bin} > a_{max}$, at some point of interaction, R_0, the binary will always be *soft*. A soft binary will not survive a scattering event and can thus not reach the SMBH intact to be disrupted by the Hills mechanism.

7.2 Resonant Relaxation

In a highly symmetric potential, like a Keplerian potential, resonant relaxation can occur due to fixed orbits coherently building up torque. This collection of torques can then change the direction and or magnitude of another orbits angular momentum. The proposal is that this collection of torques, decreases the angular momentum of a binary's orbit within 1 pc from the galactic centre, where the potential still can be assumed Keplerian (e.g. by Rauch and Tremaine (1996) and Hopman and Alexander (2006)). This decrease in angular momentum makes the binary's orbit eccentric enough so that the binary may have a close encounter with the SMBH, leading to ejection of a HVS. The eccentricity of the binary's orbit can be described as

$$e = \sqrt{1 + \frac{2 E \ell^2}{G^2 m_{bin}^3 M_{bh}^2}}, \tag{7.5}$$

where m_{bin} is the total binary mass, E is the total orbital energy (potential energy + kinetic energy), and ℓ is the angular momentum. For circular and elliptical orbits, the magnitude of the potential energy is larger than the kinetic energy, and the potential energy is negative out of the convention that work is gained at a loss of potential energy. Assuming that the energy stays constant, then decreasing the angular momentum will increase the eccentricity of the orbit. Resonant relaxation does not infer any critical physical constraints on the binary itself, and can thus relax the binaries without consuming parts of the population due to disruption in the relaxation process.

7.3 Massive Perturber

(Perets et al. (2007)) A massive perturber is a large massive body such as a giant gas cloud, stellar cluster, or even an intermediate mass black hole. Similar to two-body scattering, a massive perturber relaxes the binary by exchanging kinetic energy and momentum through gravity. However, since the mass of the massive perturber easily exceeds 100 $M_{\odot}$, the process must occur over larger distances through multiple weak interactions to not disrupt the binary. The effects of a massive perturber can be effective up to 100 pc from the galactic centre. Close interactions with a massive perturber may disrupt the binary. However, considering the large effective range of a massive perturber, the process has access to a larger binary population compared with two-body scattering and resonant relaxation.

Chapter 8

Hard vs Soft Binaries

In this chapter, I am going to determine the possibility of whether or not the observed HVS in my catalogue may have originated from hard binaries, being transported to the galactic centre through two-body scattering. Assuming the mass of the collider is 1 $M_{\odot}$, the maximum binary separation allowing for each binary to be hard at a given distance from the galactic centre can be calculated using equation (7.4). This binary separation limit is calculated for the three different binary mass ratios at three different distances, $R_0 = 0.1$, 0.3, 1 pc, marked as red, green, and blue vertical lines in each plot of the distribution of binary separation in Appendix C & D.

From e.g. Figure D.2 in Appendix D, we see from these limits that the binaries chances of surviving a two-body scattering event increases for more massive binaries, even though the binary separation increases with mass as well. Comparing equation (7.4) with equation (6.1), it is clear that a_{max} scales faster with mass of the binary than the a_{bin} does. To get a quantitative answer to the survival rate of each scattered binary, the limit separation, a_{max}, can be compared with the previously calculated distribution of a_{bin} for each binary, from which a hard fraction, f_h, can be calculated. The hard fraction is calculated for each mass ratio, q, and distances, R_0. This fraction can now tell how the probability of a HVS surviving a scattering event varies with changes in the variables R_0, q, a_{bin}, v_{ej}, and mass.

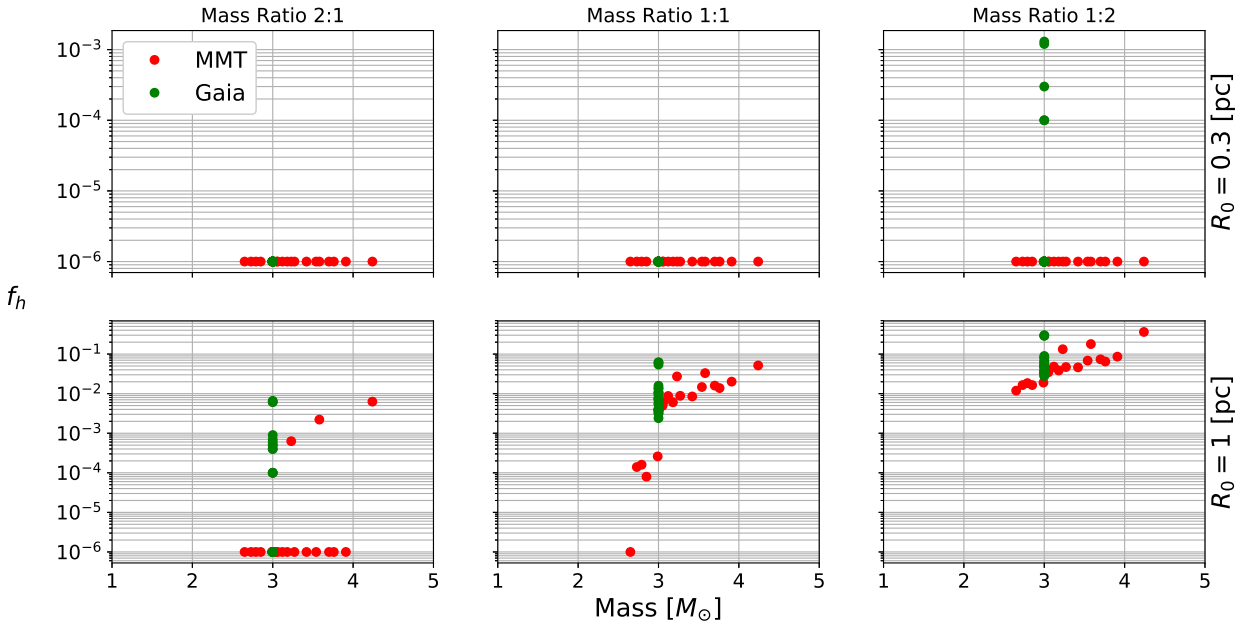

Figure 8.1: The fraction of binaries considered hard versus the mass of the primary star for the different mass ratios and distances from the galactic centre. Notice the logarithmic scale for the hard fraction, where all fractions $< 10^{-6}$ is set to equal 10^{-6} to avoid fractions close to zero ($10^{-\infty}$).

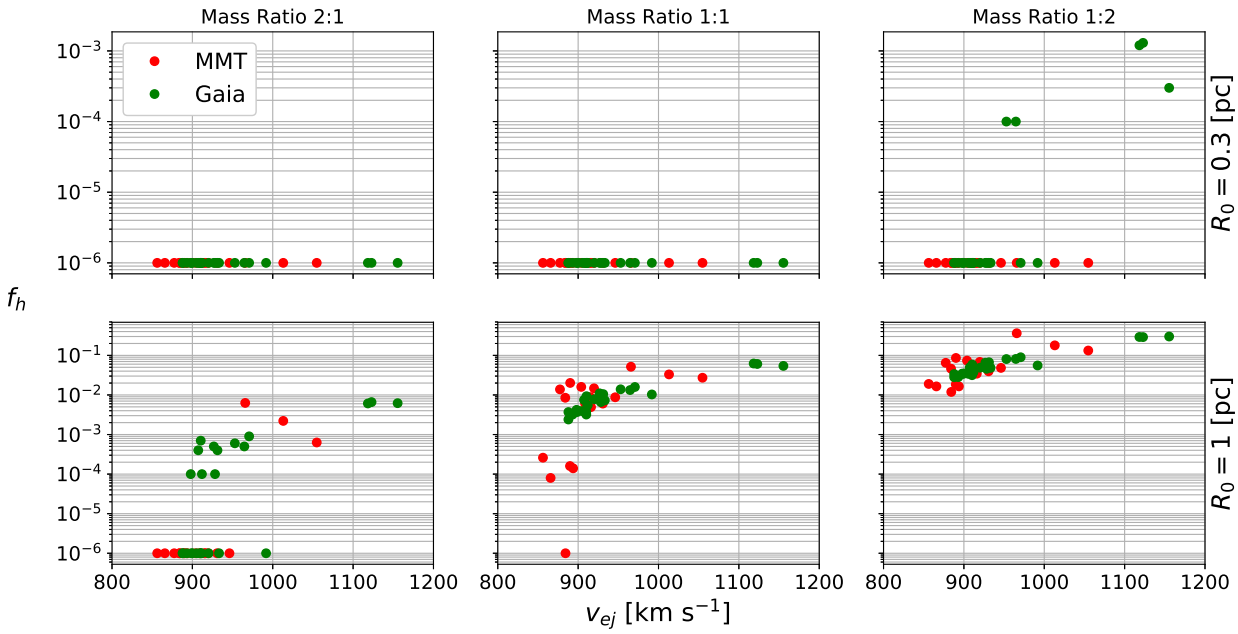

Figure 8.2: The fraction of binaries considered hard versus ejection velocity for different mass ratios and distances from the galactic centre. Notice the logarithmic scale for the hard fraction, where all fractions $< 10^{-6}$ is set to equal 10^{-6} to avoid fractions close to zero ($10^{-\infty}$).

Evidently, the hard fraction, f_h, was zero for all binaries and combinations of mass ratios at $R_0 = 0.1$ pc, meaning that all binaries scattered within 0.1 pc will be disrupted at the scattering event and can thus not produce HVS through the Hills mechanism. The reason for this is because at $R_0 = 0.1$ pc from the galactic centre, $a_{max} \lesssim 0.05$ AU for all binaries, which is physically impossible. As previously mentioned, the chances of a binary surviving a two-body scattering event increases for more massive binaries and larger distances from the galactic centre. What we also can see now in Figure 8.1, is that, for a few binaries belonging to the Gaia stars, there exists a slim chance of being considered hard even at $R_0 = 0.3$ pc. Although, this is only true for fastest stars, since $a_{bin} \propto 1/v_{ej}^2$ and $a_{max} \propto R_0$. Nonetheless, high binary mass and large distance from the galactic centre yields the most promising circumstances for a binary to be considered hard. In Figure 8.1, for a mass ratio of 1:2 and $R_0 = 1$ pc, the hard fraction ranges from $10^{-2} - 10^{0}$, from lightest to most massive binary. Stepping down to a mass ratio of 1:1 drastically decreases the hard fraction by several orders of magnitude. If we compare the same circumstances in Figure 8.2, we see that it is the binaries belonging to the slower stars, whose hard fraction decreases the most. Comparing Figure 8.1 & 8.2 for $R_0 = 1$ pc and mass ratio 2:1, the three MMT stars with the largest f_h aligns and clearly visualises the importance of how disruption through scattering decreases for higher binary masses, compared to ejection velocity.

Chapter 9

Implications of Binary Separation

From the hard fraction calculated for each binary in the previous chapter we can now quantitatively determine whether or not the observed HVS may have originated from a tidally disrupted binaries, being sent on a black hole encountering orbit as a consequence of a random two-body scattering event.

In my results, the binary with the largest hard fraction, belonging to the MMT star 'HVS 4', had a 36% chance of surviving a scattering event at 1 pc from the galactic centre for a binary with a 1:2 mass ratio. However, for the majority of the binaries, the chance of surviving was between 1-10%. In perspective, Yu and Tremaine (2003) predicted a binary disruption rate of 10^{-5} yr^{-1}, equivalent to 10 disrupted binaries every 1 Myr. This means that in best case scenario, 100-1000 binaries must be two-body scattered every 1 Myr to solely produce the observed HVS. In the age of the galaxy, $\sim 10^{10}$ yr, that is equivalent to $\geq 10^7$ scattered binaries. Bear in mind that every scattering event does not occur at 1 pc from the galactic centre, nor does it for only 1:2 mass ratio binaries, and every binary disruption does not result in an observable HVS. Furthermore, simulations made by Generozov and Madigan (2020) indicated that as many as 20-30% of binary - SMBH encounters lead to collisions with other stars instead of disruption. This means that in reality, the required two-body scattering rate is likely much higher. I assume the galactic potential within 1 pc from the galactic centre to be Keplerian, meaning that the enclosed mass of all stars is less than the mass of Sgr A*, $\sim 10^6$ $M_\odot$. Assuming the average star mass in the galactic centre is 1 $M_\odot$, my previous assumptions dictates that there are approximately 10^6 stars within 1 pc from the galactic centre. If two-body scattering truly was the only process responsible for transporting binaries towards the galactic centre, then the galactic centre would have been drained of its stars and binaries ten times over at this necessary rate of scattering.

Although, Generozov and Madigan (2020) stated that all observed S-stars captured around the SMBH have masses ranging from 8-15 $M_\odot$. If these S-stars are the captured secondary star of a tidally disrupted binary, that would indicate binaries with a mass ratio of 1:4 for the mass of the observed HVS. When calculating the hard fraction for these

hypothetical binaries, we see in Figure 9.1 that this increases the probability of a binary surviving a two-body scattering event with a magnitude of 10. This is still not large enough to solely sustain the predicted disruption rate.

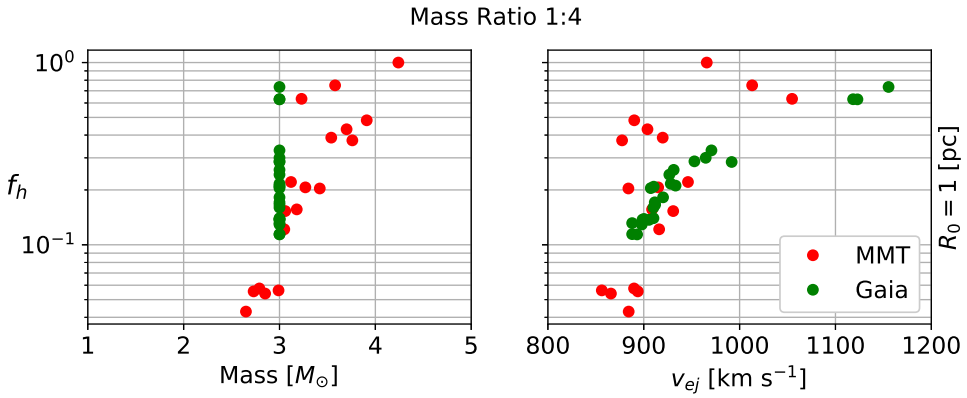

Figure 9.1: Hard fraction vs mass and ejection speed for observed HVS originating from binaries with mass ratio of 1:4, being two-body scattered at a distance $R = 1$ pc from galactic centre.

So far, no S-stars with mass below 8 $M_\odot$ have been observed due to the stars being to faint for current instruments. Since as binaries with mass ratios of 1:4 is well in the reasonable range of where ejection probability between primary or secondary binary components is equal, if binaries with 1:4 mass ratios are being tidally disrupted, S-stars with mass 2-5 $M_\odot$ should exist. The reason why no HVS with a mass of 10-15 $M_\odot$ have been observed is because their lifetime is shorter than the time it takes for them to travel to where they can be observed. For a 10-15 $M_\odot$ star being ejected at 800 km s^{-1}, assuming no deceleration due to the galactic potential, it would still take that star 10 Myr to reach our solar system which is approximately its entire life time. Even if the high mass star was ejected soon after its birth, it would not likely survive the journey through space to reach the locations where HVS have been observed.

To hypothesise that only one process is liable for the transportation of binaries is naïve. Even if the hard fraction for high mass binaries is certainly within possible limits, due to fact that two-body scattering is a random event in nature, the process is far too inefficient to expect it to be a major contributor to the relaxation process of binaries. Naturally, the stellar population increases with the distance from the galactic centre, but so does the difficulty of a successful scattering. Perets et al. (2007) found that massive perturbers could decrease the relaxation timescales with 10^1-10^7 compared to two-body scattering, alone. Because of massive perturbers large effective range of $\sim$ 100 pc from the galactic centre, where ongoing star formation takes place, massive perturber is likely responsible for the migration of massive binaries and the origin of the observed young S-stars. Similarly, Hopman and Alexander (2006) found that the steady state current of stars towards the

central SMBH was $\lesssim 10$ larger than that of two-body scattering, alone. However, resonant relaxation cannot solely explain the existence of the S-stars because some process must have transported the S-stars within the effective range of resonant relaxation in the first place.

Chapter 10

Future Advancements

If this project where to be repeated, there are some improvements I would make that would allow for a more detailed analysis. First and foremost, the mass of the Gaia stars has to be determined. With isochronic fitting and the age of the star, the star's spectral properties, colour and apparent magnitude, can be corrected for the stellar evolution and the mass can be determined. Secondly, the observed radial velocity of the MMT stars is only transformed into galactic rest frame. The total velocity of the MMT stars could be determined by integrating their total velocity in the galactic potential by Paczynski (1990), and solved for the missing tangential component using equation (5.1). Further more, multiple variables in the analysis have been assumed or ignored out of simplicity, such as eccentricity of the binary components orbit, the rotational direction of the binaries when approaching the SMBH (prograde or retrograde), and the inclination of the binaries. Finally, a more updated model of the galactic potential might be advised. The results calculated with the model of the galactic potential by Paczynski (1990) showed agreement with previous works. Still, future works might suggest a different approach, depending on where in the galaxy future HVS are observed. For a HVS detected within 4 kpc from the galactic centre, it would be advised to use a model more focused on describing the potential of the galactic bulge and disk.

Highly desirable future discoveries are low mass S-stars with low eccentric orbits accompanied by high mass HVS to confirm high mass binary disruption through the Hills mechanism. Future observations of the binary population near the galactic centre, and properties of observed S-stars, will allow for further conclusions about the different relaxation processes near the galactic centre. If the observed S-stars were to be traced back to place of origin, responsible relaxation process could be determined from the combined works of Generozov and Madigan (2020), Hopman and Alexander (2006), and Perets et al. (2007).

Chapter 11

Conclusion

From a collection of observed HVS, I have calculated the properties of the original binaries prior to being tidally disrupted through the Hills Mechanism. From the properties of the original binaries, I have tried to determine whether or not these binaries have been sent on black hole encountering orbits by means of two-body scattering. My findings are summarised as follows:

1. To increase a binary's chances of surviving a two-body scattering event, the most important property of the binary is to have sufficiently large mass. It is equally important that the scattering event occurs as far out from the galactic centre as possible. In fact, no binaries within 0.1 pc from the galactic centre could two-body scattered without being disrupted at the scattering event. Two-body scattering within 0.1 pc from the galactic centre requires a maximum binary separation smaller than what is possible because of the binary components physical size.

2. Two-body scattering of lower mass binaries is an extremely inefficient process. More than 100 binaries need to scatter every 1 Myr to solely sustain the disruption rate of 10^{-5} yr^{-1}, suggested by Yu and Tremaine (2003). During the Milky Way's life time, $\sim 10^{10}$ yr, the estimated star population of $\sim 10^{6}$ stars within 1 pc from the galactic centre would all need to be scattered ten times over at this scattering rate. This indicates that binaries originating from within 1 pc from the galactic centre have most likely been transported by resonant relaxation, as suggested by Hopman and Alexander (2006).

3. The hard fraction of binaries with a mass ratio of 1:4 was a magnitude of 10 larger than that of binaries with mass ratio 1:2, meaning that the required scattering rate is instead 10 binaries every 1 Myr. This is still not efficient enough to solely sustain the expected disruption rate. Therefore, I suspect that the observed S-stars have originated from high mass binaries that have been transported by multiple weak interactions with a massive perturber, as suggested by Perets et al. (2007). Still, the hard fraction of these high mass S-star binaries are large enough to not completely rule out two-body scattering as the transportation method of individual HVS.

Bibliography

Bromley, B. C., Kenyon, S. J., Brown, W. R., and Geller, M. J. (2018). Nearby High-speed Stars in Gaia DR2. *ApJ*, 868(1):25.

Bromley, B. C., Kenyon, S. J., Geller, M. J., Barcikowski, E., Brown, W. R., and Kurtz, M. J. (2006). Hypervelocity Stars: Predicting the Spectrum of Ejection Velocities. *ApJ*, 653(2):1194–1202.

Brown, W. R., Geller, M. J., and Kenyon, S. J. (2012). MMT Hypervelocity Star Survey. II. Five New Unbound Stars. *ApJ*, 751(1):55.

Brown, W. R., Geller, M. J., and Kenyon, S. J. (2014). MMT Hypervelocity Star Survey. III. The Complete Survey. *ApJ*, 787(1):89.

Brown, W. R., Geller, M. J., Kenyon, S. J., and Kurtz, M. J. (2005). Discovery of an Unbound Hypervelocity Star in the Milky Way Halo. *ApJ*, 622(1):L33–L36.

Brown, W. R., Lattanzi, M. G., Kenyon, S. J., and Geller, M. J. (2018). Gaia and the Galactic Center Origin of Hypervelocity Stars. *ApJ*, 866(1):39.

Generozov, A. and Madigan, A.-M. (2020). The Hills Mechanism and the Galactic Center S–stars. *arXiv e-prints*, page arXiv:2002.10547.

Gualandris, A. and Portegies Zwart, S. (2007). A hypervelocity star from the Large Magellanic Cloud. *MNRAS*, 376(1):L29–L33.

Hills, J. G. (1988). Hyper-velocity and tidal stars from binaries disrupted by a massive Galactic black hole. *Nature*, 331(6158):687–689.

Hopman, C. and Alexander, T. (2006). Resonant Relaxation near a Massive Black Hole: The Stellar Distribution and Gravitational Wave Sources. *ApJ*, 645(2):1152–1163.

Kreuzer, S., Irrgang, A., and Heber, U. (2020). Hypervelocity Stars in the Gaia era. Revisiting the most extreme stars from the MMT survey. *arXiv e-prints*, page arXiv:2003.12766.

Miyamoto, M. and Nagai, R. (1975). Three-dimensional models for the distribution of mass in galaxies. *PASJ*, 27:533–543.

Paczynski, B. (1990). A Test of the Galactic Origin of Gamma-Ray Bursts. *ApJ*, 348:485.

Perets, H. B., Hopman, C., and Alexander, T. (2007). Massive Perturber-driven Interactions between Stars and a Massive Black Hole. *ApJ*, 656(2):709–720.

Rauch, K. P. and Tremaine, S. (1996). Resonant relaxation in stellar systems. *NewA*, 1(2):149–170.

Sari, R., Kobayashi, S., and Rossi, E. M. (2010). Hypervelocity Stars and the Restricted Parabolic Three-Body Problem. *ApJ*, 708(1):605–614.

Svensson, K. M., Church, R. P., and Davies, M. B. (2008). The nature of hypervelocity stars as inferred from their Galactic trajectories. *MNRAS*, 383(1):L15–L19.

Yu, Q. and Tremaine, S. (2003). Ejection of Hypervelocity Stars by the (Binary) Black Hole in the Galactic Center. *ApJ*, 599(2):1129–1138.

Appendix A

Catalogue of Observed Hypervelocity Stars

Table A.1: Tabulated data from Brown et al. (2014), from which all further results have been derived from. (ℓ, b) taken from Brown et al. (2012)

HVS	**MMT** Designation	(ℓ, b) [deg]	R_g [kpc]	v_g [km s^{-1}]	M [$M_\odot$]
1	SDSS J090744.99+024506.89	(227.33, 31.33)	107 ± 15	673.1	3.23 ± 0.13
4	SDSS J091301.01+305119.83	(194.76, 42.56)	70 ± 10	551.5	4.24 ± 0.16
5	SDSS J091759.47+672238.35	(146.23, 38.70)	50 ± 5	650.1	3.58 ± 0.11
6	SDSS J110557.45+093439.47	(243.12, 59.56)	58 ± 7	501.4	3.06 ± 0.11
7	SDSS J113312.12+010824.87	(263.83, 57.95)	53 ± 6	402.0	3.76 ± 0.12
8	SDSS J094214.03+200322.07	(211.70, 46.33)	58 ± 10	408.3	3.42 ± 0.20
9	SDSS J094214.03+200322.07	(244.63, 44.38)	77 ± 12	458.8	3.54 ± 0.16
10	SDSS J120337.85+180250.35	(249.93, 75.72)	53 ± 6	416.7	2.65 ± 0.11
12	SDSS J105009.59+031550.67	(247.11, 52.46)	67 ± 8	416.5	2.73 ± 0.14
13	SDSS J105248.30−000133.94	(251.65, 50.64)	107 ± 19	423.9	3.05 ± 0.18
14	SDSS J104401.75+061139.02	(241.78, 53.20)	105 ± 16	409.4	3.18 ± 0.15
15	SDSS J113341.09−012114.25	(266.51, 55.92)	67 ± 10	328.3	2.99 ± 0.12
16	SDSS J122523.40+052233.84	(285.86, 67.38)	71 ± 12	346.2	2.85 ± 0.15
17	SDSS J164156.39+472346.12	(73.52, 41.16)	49 ± 4	435.8	3.91 ± 0.09
18	SDSS J232904.94+330011.47	(103.64, -26.77)	80 ± 11	446.2	3.27 ± 0.12
19	SDSS J113517.75+080201.49	(256.05, 63.74)	98 ± 15	492.0	3.12 ± 0.17
20	SDSS J113637.13+033106.84	(262.56, 60.39)	76 ± 11	396.6	2.79 ± 0.12
21	SDSS J103418.25+481134.57	(165.26, 56.11)	113 ± 21	391.9	3.70 ± 0.21

Table A.2: Tabulated data from Bromley et al. (2018), from which all further results have been derived from.

Gaia **DR2** Designation	(ℓ, b) [deg]	ω [mas]	R_g [kpc]	v_g [km s^{-1}]
5932173855446728064	(329.9, -2.7)	0.454 ± 0.029	6.2 ± 0.1	747 ± 3
1383279090527227264	(65.5, 48.8)	0.118 ± 0.016	10.0 ± 0.9	924 ± 168
1478837543019912064	(59.0, 71.9)	0.105 ± 0.019	11.4 ± 1.6	876 ± 230
6456587609813249536	(338.3, -40.9)	0.099 ± 0.019	7.3 ± 1.7	889 ± 250
6492391900201222656	(324.6, -54.4)	0.095 ± 0.018	9.7 ± 1.8	678 ± 189
4326973843264734208	(2.6, 21.5)	0.199 ± 0.031	3.8 ± 0.4	730 ± 159
5846998984508676352	(309.3, -7.4)	0.095 ± 0.019	8.3 ± 1.9	671 ± 189
2089995308886282880	(60.7, 15.2)	0.071 ± 0.013	12.6 ±2.8	605 ± 144
5802638672467252736	(317.9, -19.1)	0.101 ± 0.015	7.2 ±1.1	648 ± 135
2095397827987170816	(63.0, 19.9)	0.066 ± 0.012	13.7 ± 2.9	585 ± 142
6431596947468407552	(324.2, -22.7)	0.084 ± 0.016	8.0 ± 2.2	605 ± 84
2159020415489897088	(90.5, 28.1)	0.134 ± 0.026	11.0 ± 1.3	588 ± 134
5919596571872806272	(336.2, -13.5)	0.120 ± 0.022	3.8 ± 0.9	684 ± 188
2121857472227927168	(75.5, 24.7)	0.072 ± 0.013	14.4 ± 2.6	550 ± 114
5839686407534279808	(308.0, -9.9)	0.138 ± 0.020	6.8 ± 0.5	626 ± 123
2112308930997657728	(67.0, 24.2)	0.167 ± 0.022	8.1 ± 0.4	601 ± 100
6656557095228727936	(344.2, -23.4)	0.105 ± 0.020	4.5 ±1.5	661 ± 187
5399966178291369728	(281.2, 20.8)	0.100 ± 0.017	11.7 ± 1.6	564 ± 117
4366218814874247424	(17.5, 22.3)	0.139 ± 0.021	3.8 ± 0.3	651 ± 108
5217818333256869376	(289.7, -16.2)	0.118 ± 0.018	9.6 ± 1.0	578 ± 105
6124121132097402368	(321.1, 27.7)	0.120 ± 0.024	6.4 ± 1.2	619 ± 188
2106519830479009920	(76.2, 17.4)	0.123 ± 0.018	10.0 ± 0.9	567 ± 82
5835015235520194944	(327.4, -5.6)	0.118 ± 0.020	4.7 ± 0.9	647 ± 166
1989862986804105344	(103.4, -6.3)	0.095 ± 0.016	14.6 ± 1.8	531 ± 108
5779919841659989120	(311.9, -17.5)	0.094 ± 0.016	8.3 ± 1.5	571 ± 128

Appendix B

Table of Calculated Results

Table B.1: The given uncertainties are 1σ.

HVS	**MMT** Designation	R [kpc]	z [kpc]	v_{ej} [km s^{-1}]
1	SDSS J090744.99+024506.89	92.9 ± 12.8	53.1 ± 7.8	1055 $^{+5}_{-5}$
4	SDSS J091301.01+305119.83	55.0 ± 7.4	43.3 ± 6.8	966 $^{+5}_{-6}$
5	SDSS J091759.47+672238.35	41.6 ± 3.9	27.8 ± 3.1	1013 $^{+3}_{-4}$
6	SDSS J110557.45+093439.47	32.6 ± 3.5	48.0 ± 6.1	931 $^{+4}_{-5}$
7	SDSS J113312.12+010824.87	29.5 ±3.1	44.0 ± 5.1	877 $^{+4}_{-5}$
8	SDSS J094214.03+200322.07	43.6 ± 6.9	38.3 ± 7.3	884 $^{+7}_{-8}$
9	SDSS J094214.03+200322.07	56.9 ±8.6	51.9 ± 8.4	920 $^{+6}_{-7}$
10	SDSS J120337.85+180250.35	17.2 ± 1.4	50.1 ± 5.9	884 $^{+4}_{-5}$
12	SDSS J105009.59+031550.67	43.1 ± 4.8	51.3 ± 6.4	894 $^{+5}_{-5}$
13	SDSS J105248.30−000133.94	69.6 ±12.0	81.3 ± 14.7	916 $^{+6}_{-8}$
14	SDSS J104401.75+061139.02	65.5 ±9.6	82.0 ± 12.8	909 $^{+6}_{-7}$
15	SDSS J113341.09−012114.25	38.4 ± 5.5	54.9 ± 8.3	856 $^{+6}_{-7}$
16	SDSS J122523.40+052233.84	26.4 ±4.5	65.9 ± 11.1	866 $^{+7}_{-8}$
17	SDSS J164156.39+472346.12	36.3 ±3.0	33.0 ± 2.7	890 $^{+3}_{-4}$
18	SDSS J232904.94+330011.47	71.9 ±9.8	-35.1 ± 5.0	915 $^{+5}_{-6}$
19	SDSS J113517.75+080201.49	45.4 ±6.6	86.8 ± 13.5	946 $^{+5}_{-6}$
20	SDSS J113637.13+033106.84	38.9 ± 5.4	65.3 ± 9.6	890 $^{+6}_{-6}$
21	SDSS J103418.25+481134.57	68.3 ± 11.7	90.1 ± 17.5	904 $^{+7}_{-8}$

Table B.2: The uncertainties given are 1σ.

Gaia **DR2** Designation	R [kpc]	z [kpc]	v_{ej} [km s^{-1}]	
5932173855446728064	6.2 ± 0.0	-0.1 ± 0.0	991	$^{+2}_{-2}$
1383279090527227264	7.6 ± 0.0	6.4 ± 0.2	1155	$^{+139}_{-130}$
1478837543019912064	7.0 ± 0.0	9.1 ± 0.3	1122	$^{+188}_{-169}$
6456587609813249536	3.0 ± 0.0	-6.6 ± 0.3	1118	$^{+208}_{-188}$
6492391900201222656	4.7 ± 0.0	-8.6 ± 0.3	970	$^{+141}_{-122}$
4326973843264734208	3.3 ± 0.1	1.8 ± 0.1	964	$^{+125}_{-113}$
5846998984508676352	8.2 ± 0.3	-1.4 ± 0.1	952	$^{+143}_{-124}$
2089995308886282880	11.9 ± 0.4	3.7 ± 0.1	928	$^{+101}_{-88}$
5802638672467252736	6.4 ± 0.2	-3.2 ± 0.1	933	$^{+99}_{-89}$
2095397827987170816	12.8 ± 0.4	5.2 ± 0.2	920	$^{+98}_{-85}$
6431596947468407552	6.5 ± 0.3	-4.6 ± 0.2	910	$^{+60}_{-55}$
2159020415489897088	10.4 ± 0.2	3.5 ± 0.1	911	$^{+93}_{-81}$
5919596571872806272	3.3 ± 0.1	-1.9 ± 0.1	931	$^{+147}_{-129}$
2121857472227927168	13.1 ± 0.4	5.8 ± 0.2	900	$^{+75}_{-66}$
5839686407534279808	6.7 ± 0.1	-1.2 ± 0.0	911	$^{+89}_{-80}$
2112308930997657728	7.7 ± 0.0	2.5 ± 0.1	905	$^{+70}_{-63}$
6656557095228727936	2.4 ± 0.2	-3.8 ± 0.1	926	$^{+143}_{-125}$
5399966178291369728	11.1 ± 0.2	3.6 ± 0.1	898	$^{+79}_{-69}$
4366218814874247424	2.6 ± 0.1	2.7 ± 0.1	910	$^{+81}_{-74}$
5217818333256869376	9.3 ± 0.2	-2.4 ± 0.1	897	$^{+72}_{-65}$
6124121132097402368	5.2 ± 0.1	3.9 ± 0.2	910	$^{+138}_{-117}$
2106519830479009920	9.7 ± 0.1	2.4 ± 0.1	893	$^{+55}_{-50}$
5835015235520194944	4.6 ± 0.1	-0.8 ± 0.0	907	$^{+126}_{-111}$
1989862986804105344	14.6 ± 0.3	-1.2 ± 0.0	876	$^{+69}_{-61}$
5779919841659989120	7.7 ± 0.2	-3.2 ± 0.1	887	$^{+89}_{-78}$

Appendix C

Distribution of Binary Separation of Gaia Stars

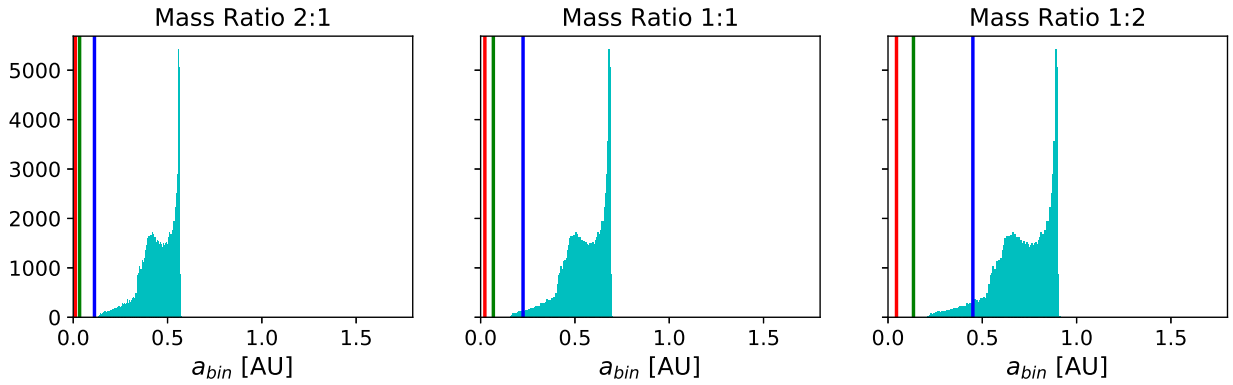

Figure C.1: Gaia 5932173855446728064

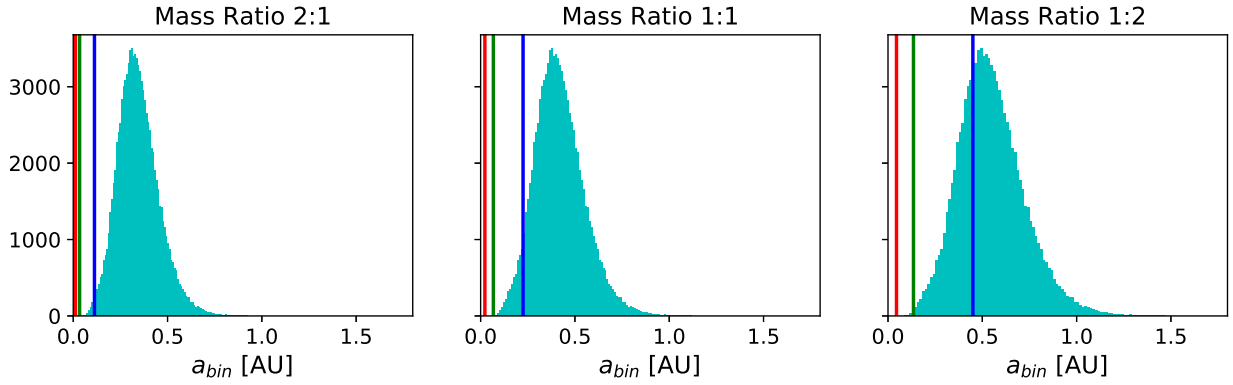

Figure C.2: Gaia 1383279090527227264

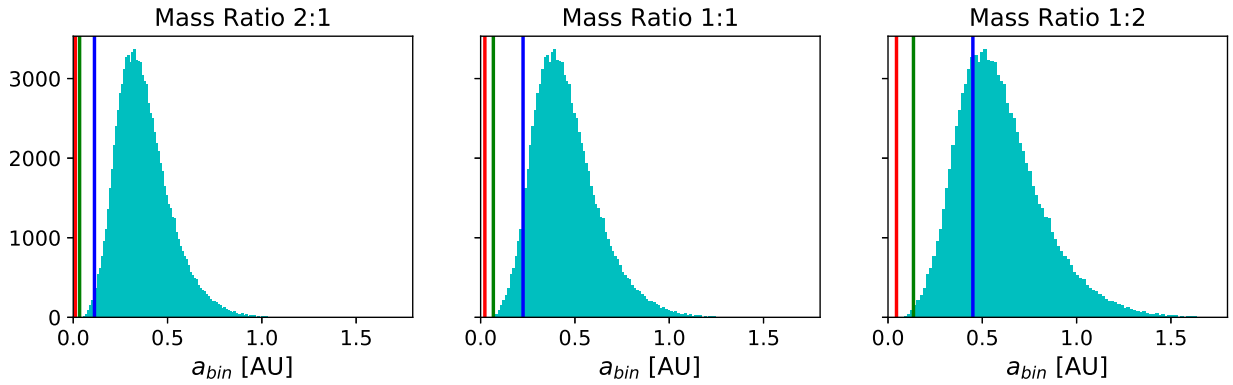

Figure C.3: Gaia 1478837543019912064

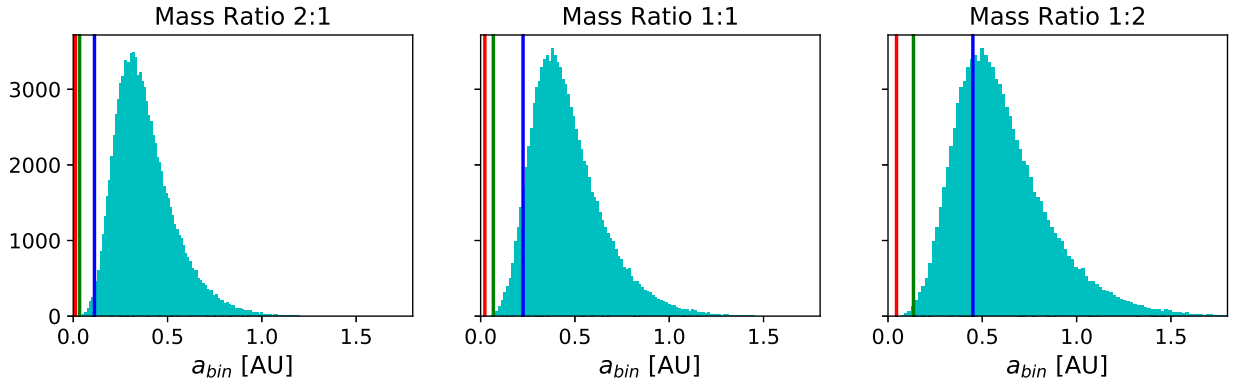

Figure C.4: Gaia 6456587609813249536

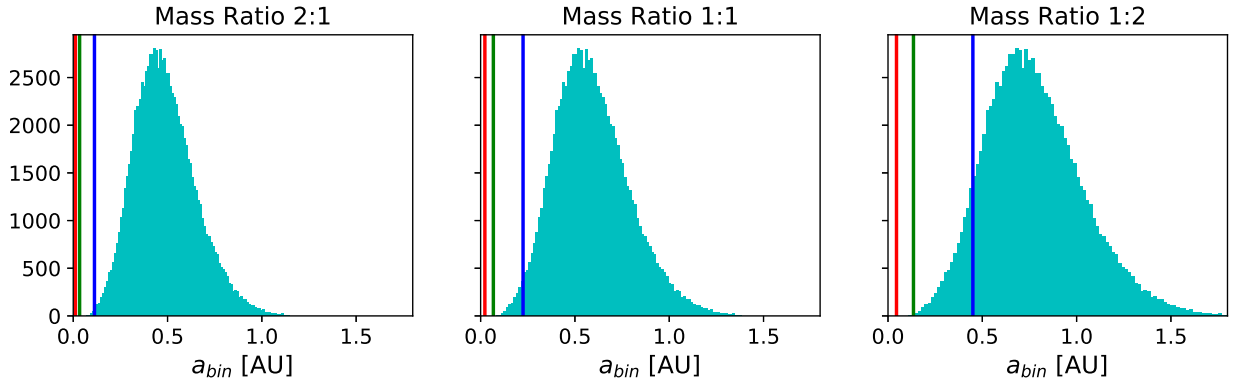

Figure C.5: Gaia 6492391900201222656

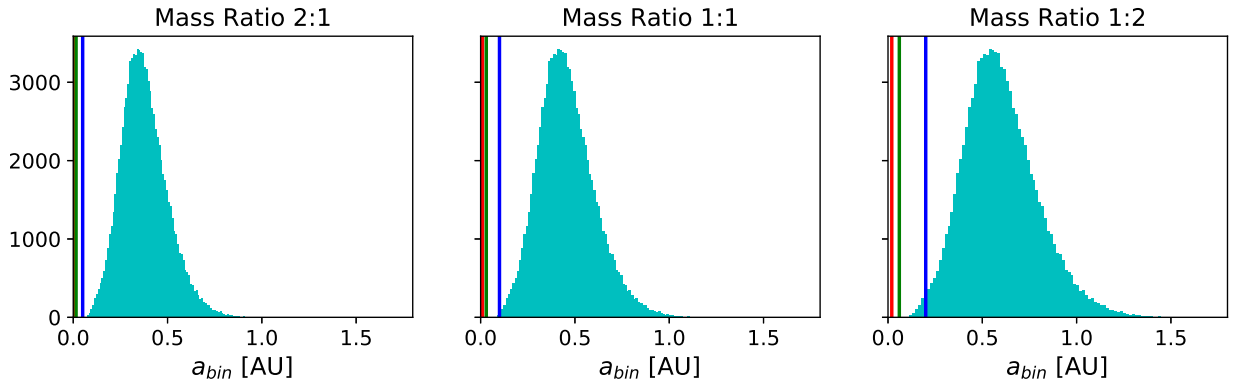

Figure C.6: Gaia 4326973843264734208

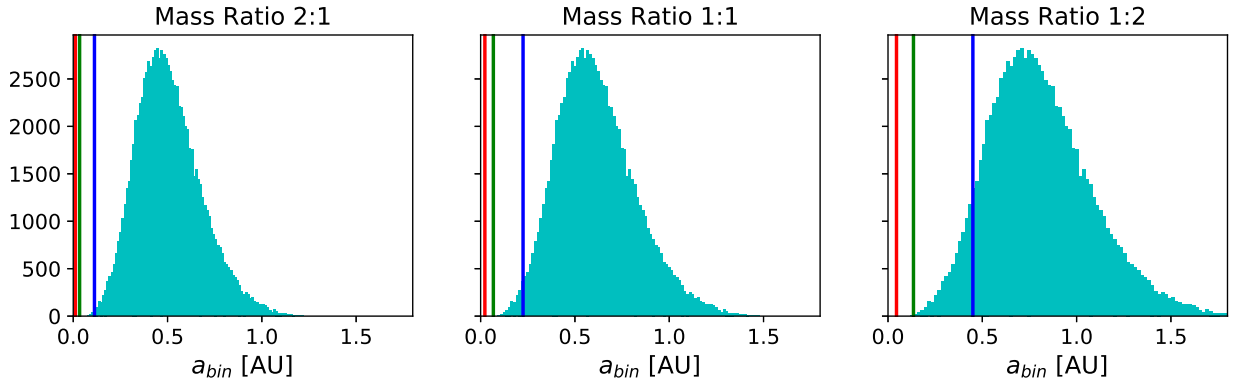

Figure C.7: Gaia 5846998984508676352

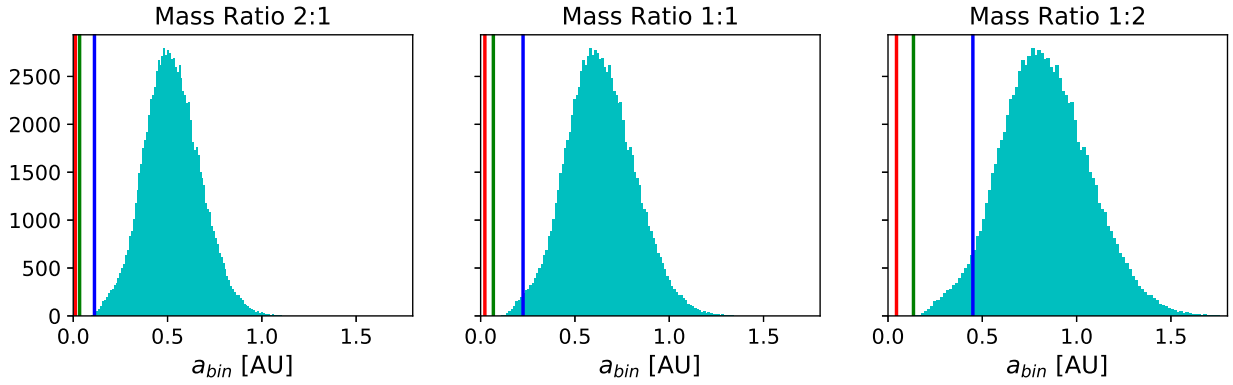

Figure C.8: Gaia 2089995308886282880

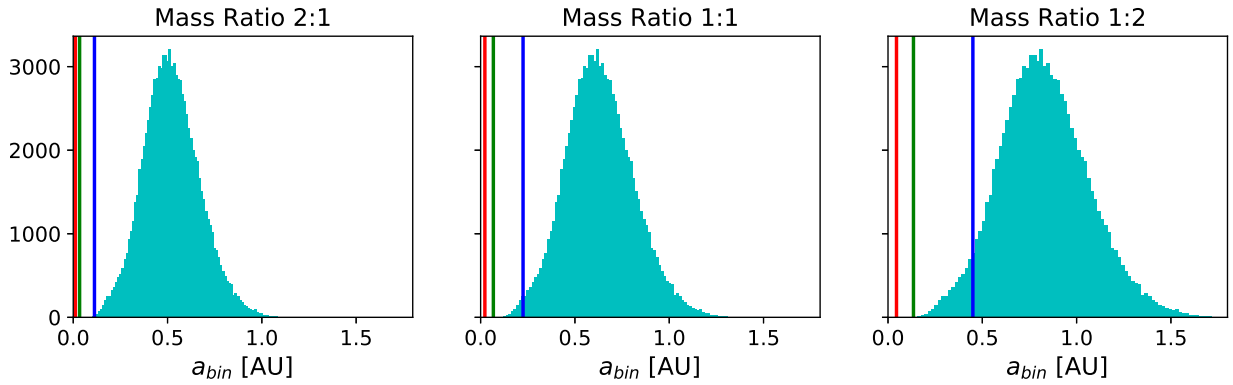

Figure C.9: Gaia 5802638672467252736

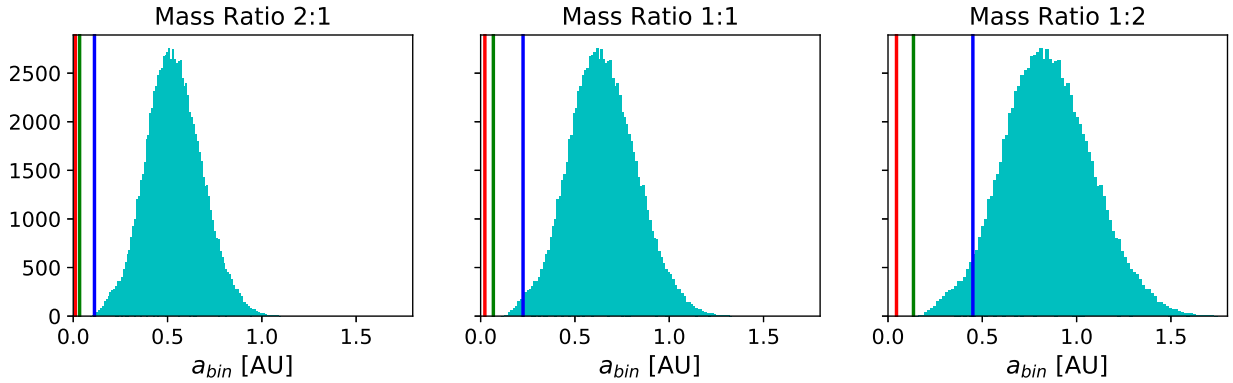

Figure C.10: Gaia 2095397827987170816

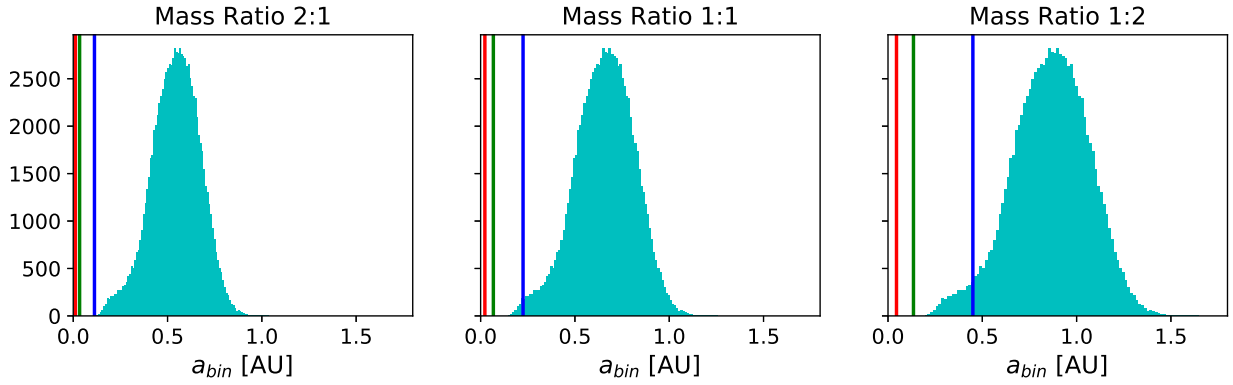

Figure C.11: Gaia 6431596947468407552

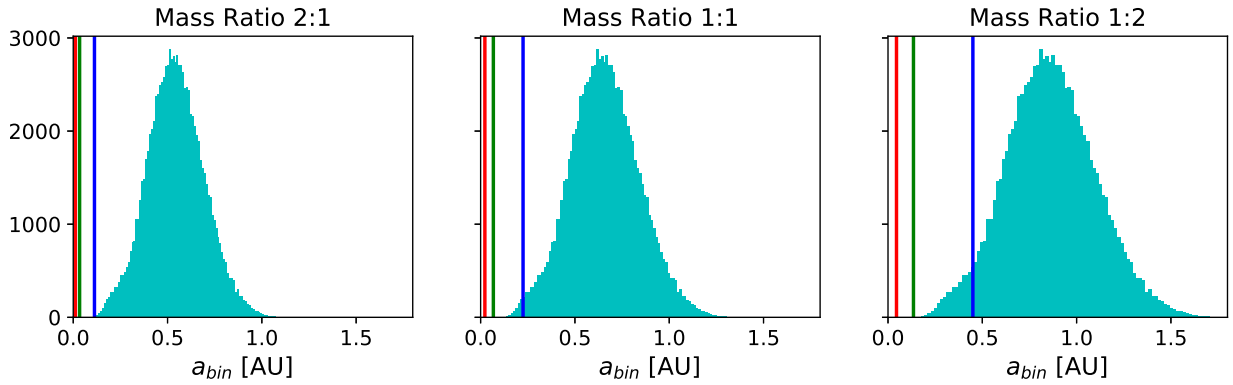

Figure C.12: Gaia 2159020415489897088

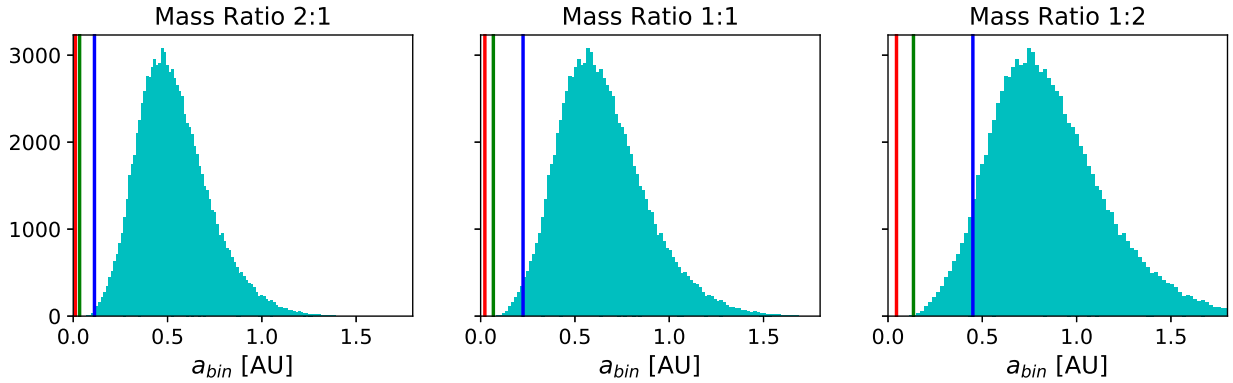

Figure C.13: Gaia 5919596571872806272

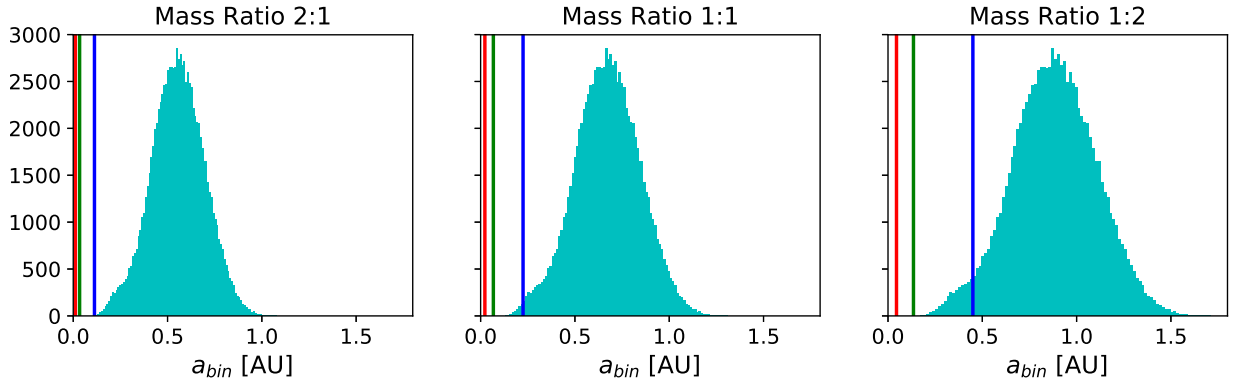

Figure C.14: Gaia 2121857472227927168

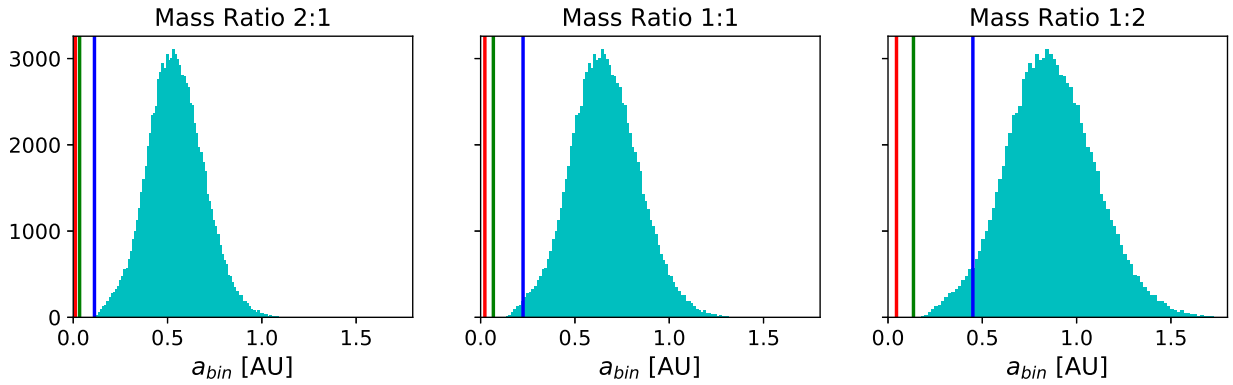

Figure C.15: Gaia 5839686407534279808

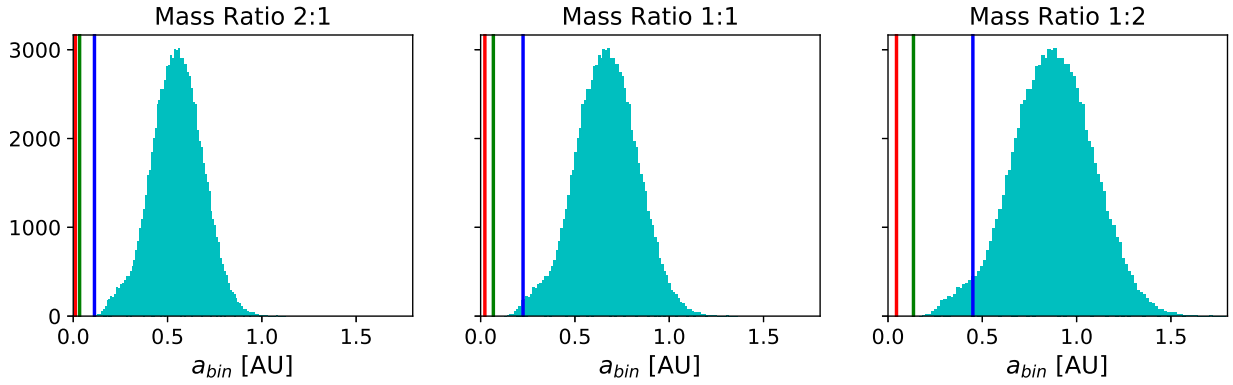

Figure C.16: Gaia 2112308930997657728

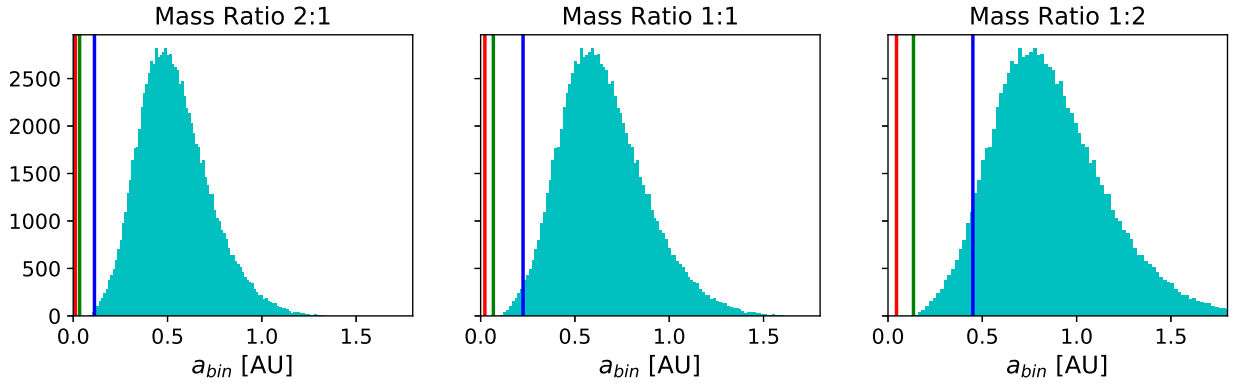

Figure C.17: Gaia 6656557095228727936

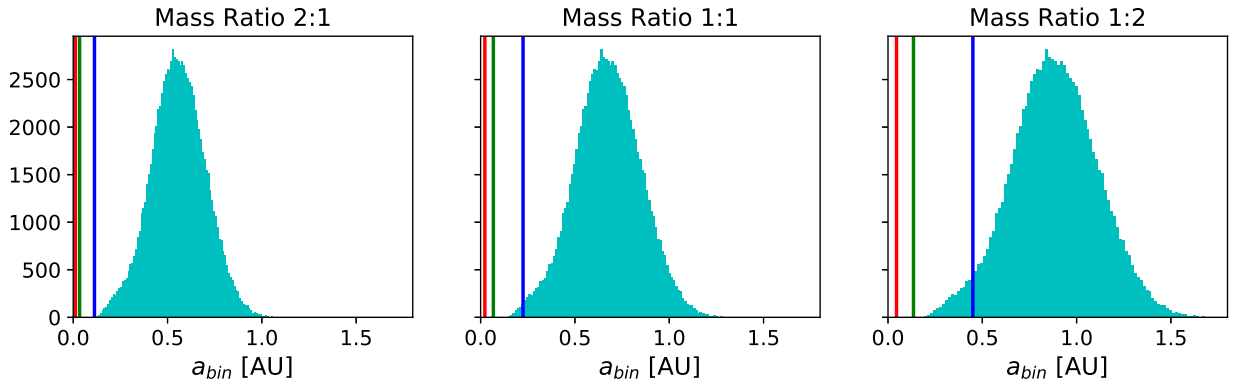

Figure C.18: Gaia 5399966178291369728

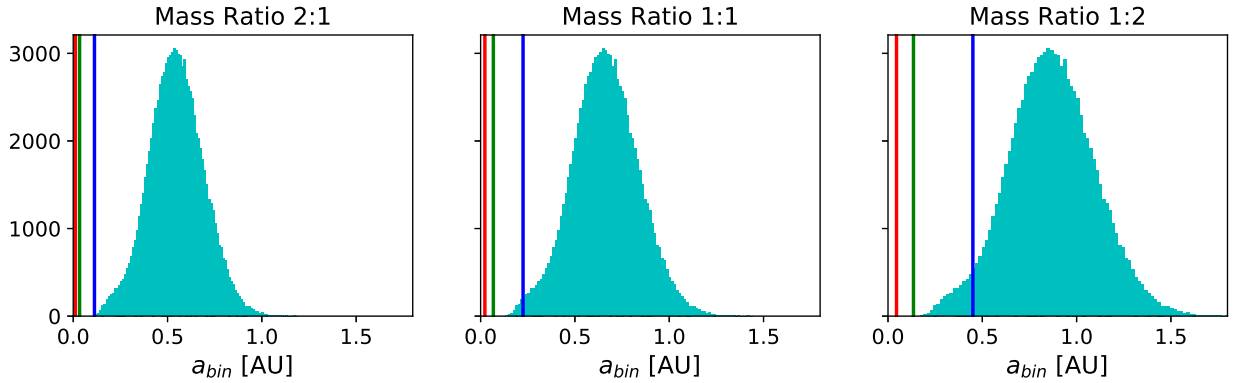

Figure C.19: Gaia 4366218814874247424

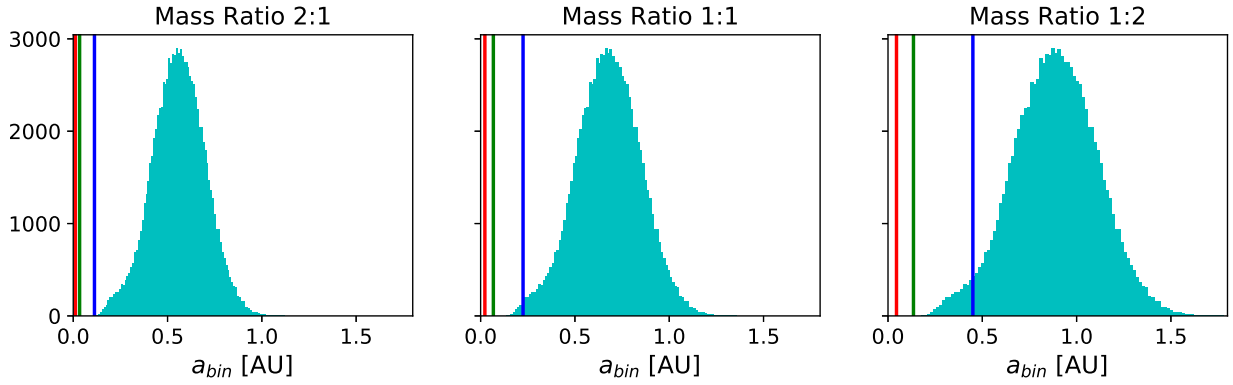

Figure C.20: Gaia 5217818333256869376

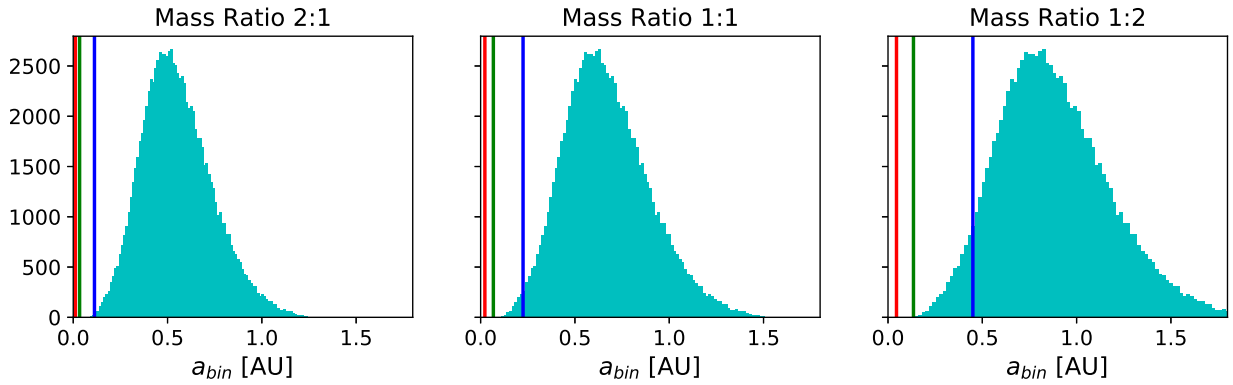

Figure C.21: Gaia 6124121132097402368

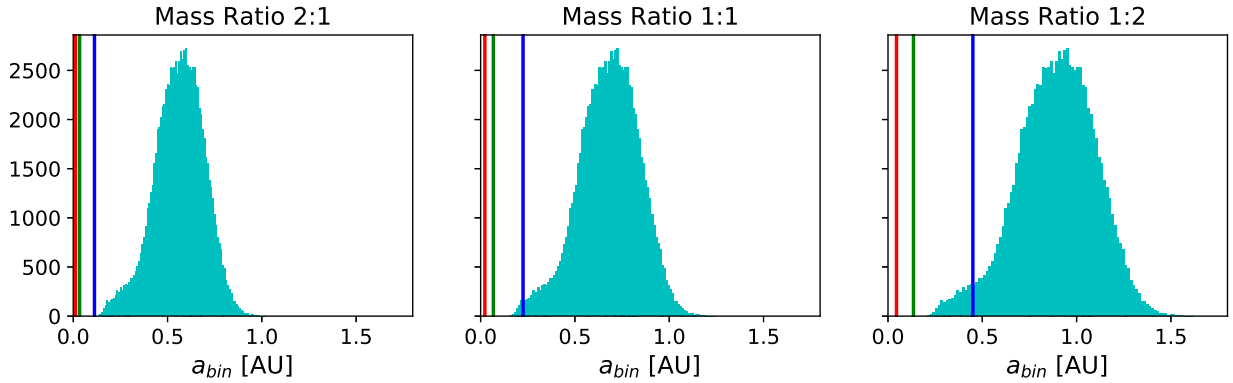

Figure C.22: Gaia 2106519830479009920

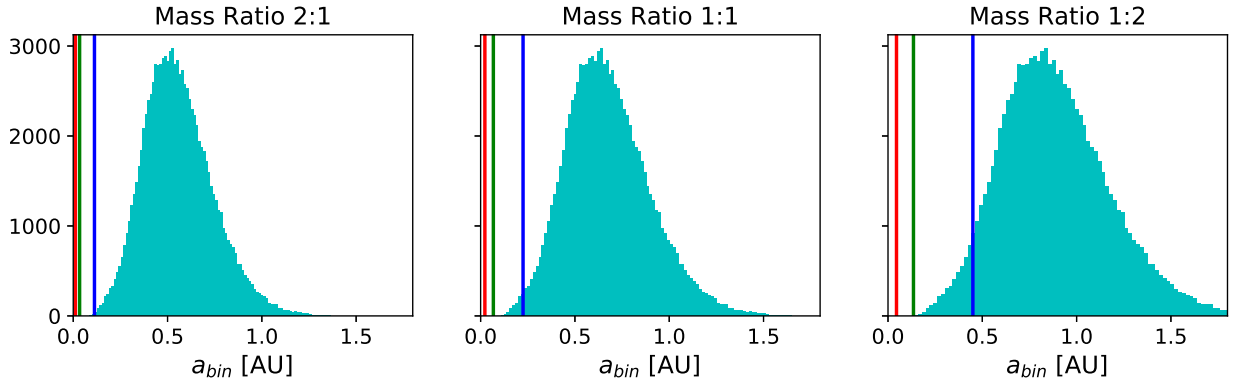

Figure C.23: Gaia 5835015235520194944

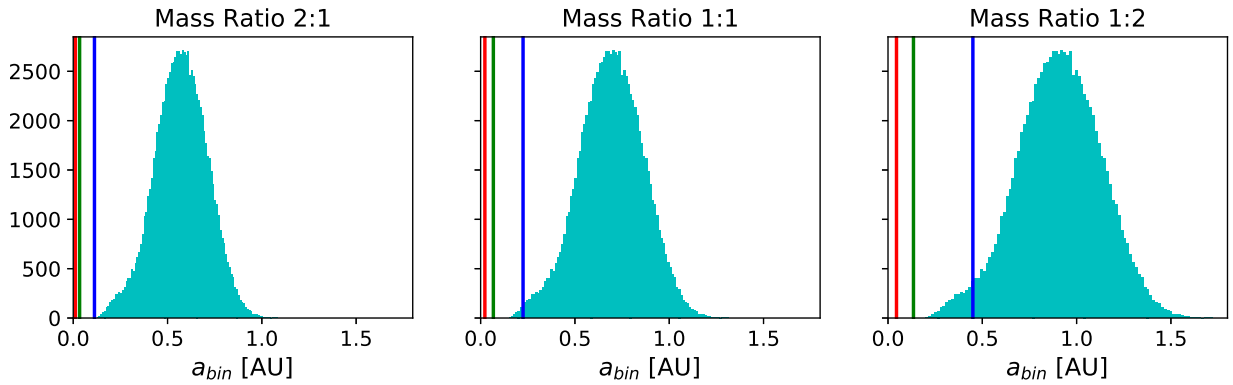

Figure C.24: Gaia 1989862986804105344

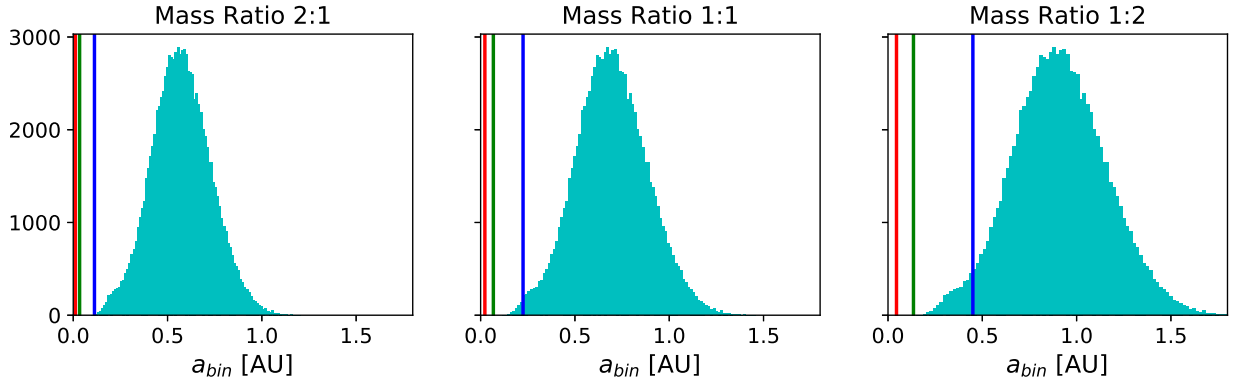

Figure C.25: Gaia 5779919841659989120

Appendix D

Distribution of Binary Separation of MMT Stars

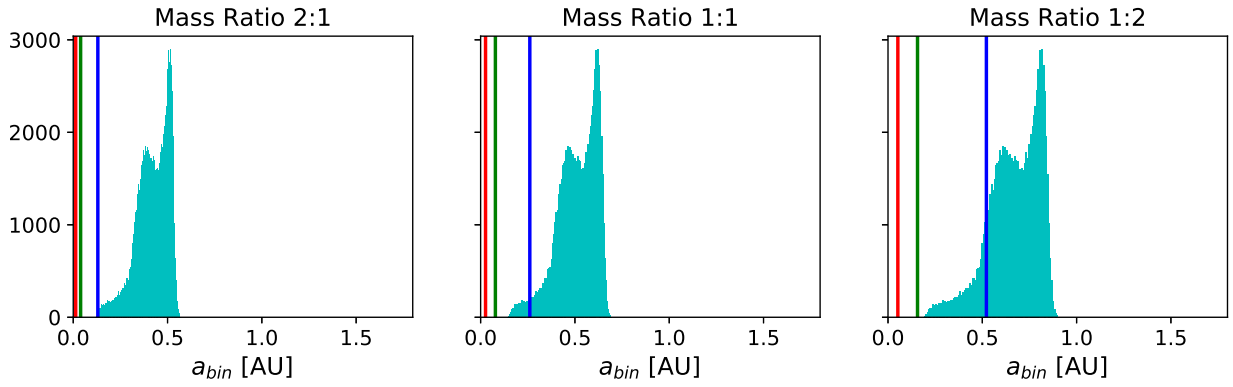

Figure D.1: HVS 1

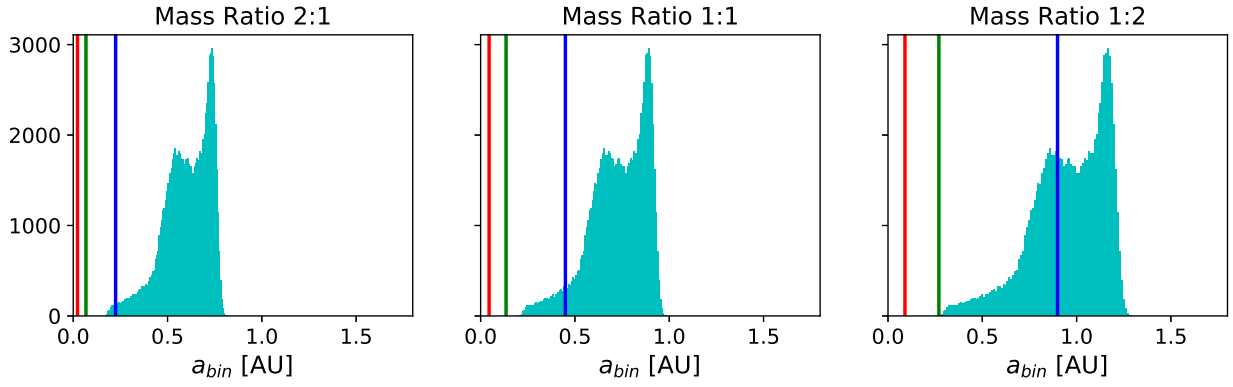

Figure D.2: HVS 4

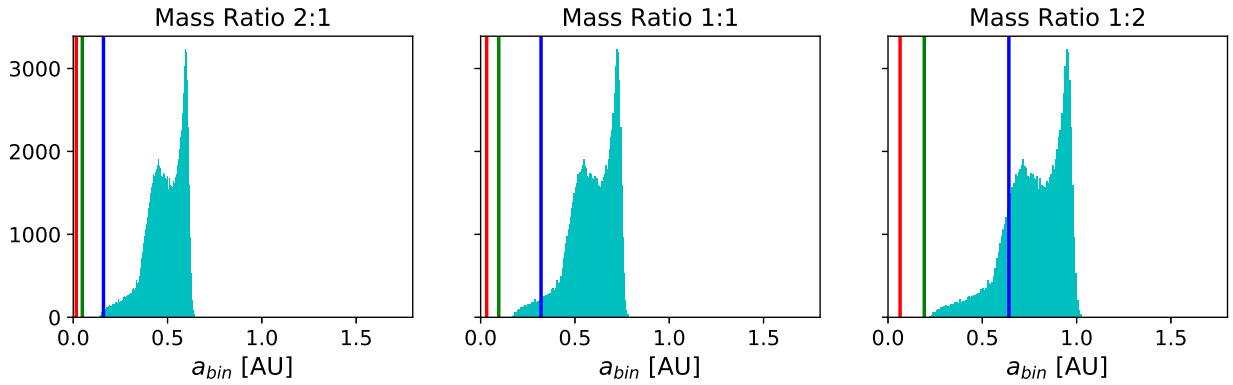

Figure D.3: HVS 5

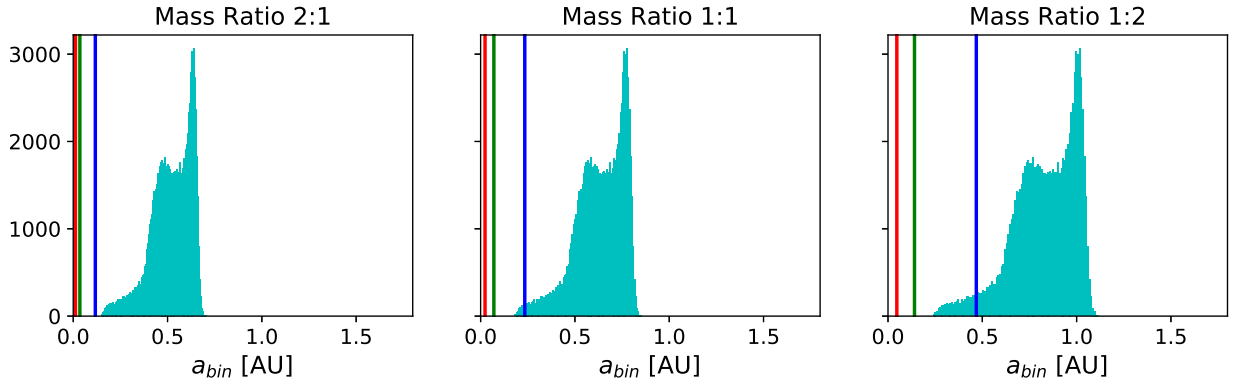

Figure D.4: HVS 6

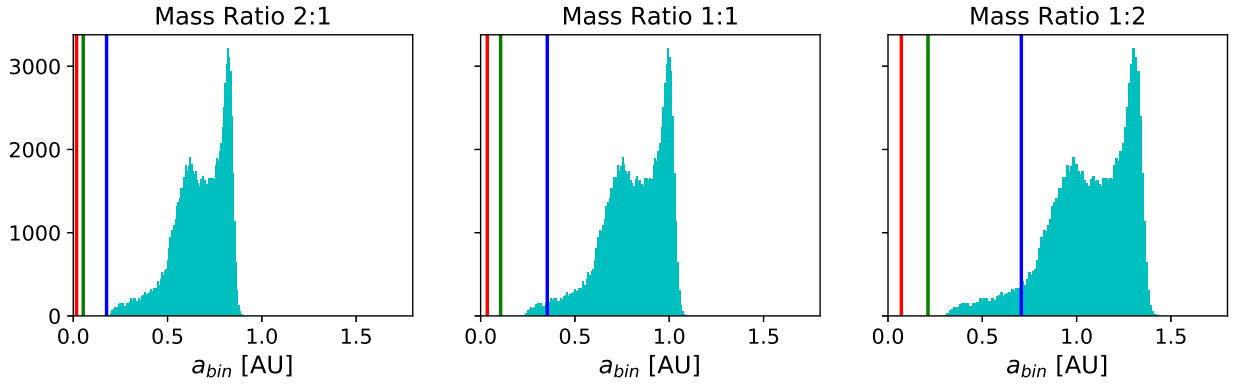

Figure D.5: HVS 7

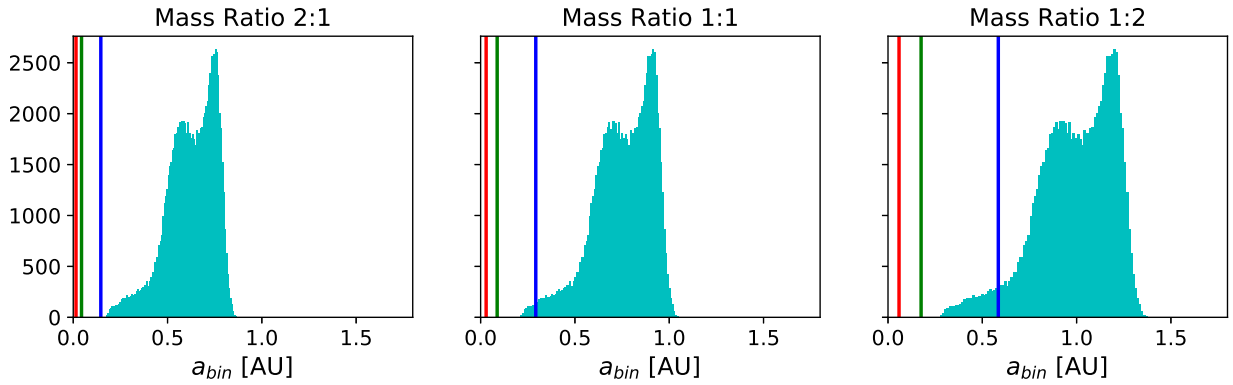

Figure D.6: HVS 8

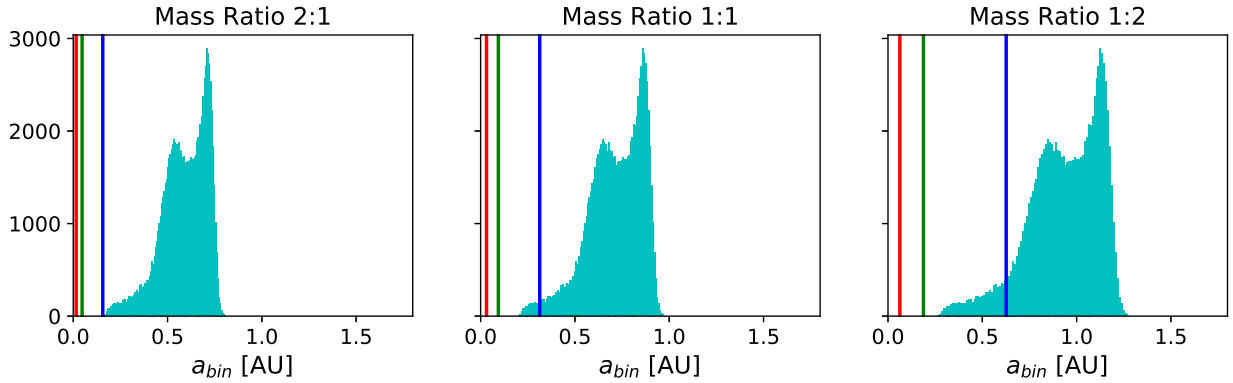

Figure D.7: HVS 9

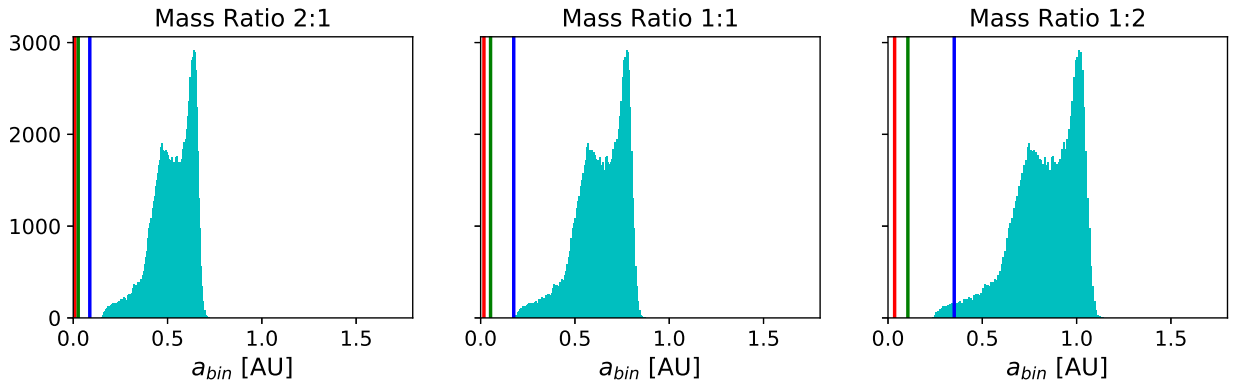

Figure D.8: HVS 10

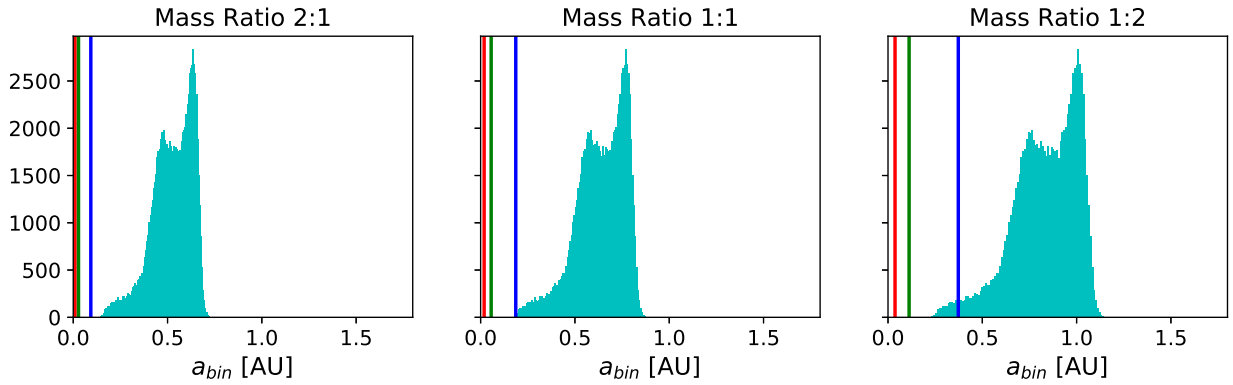

Figure D.9: HVS 12

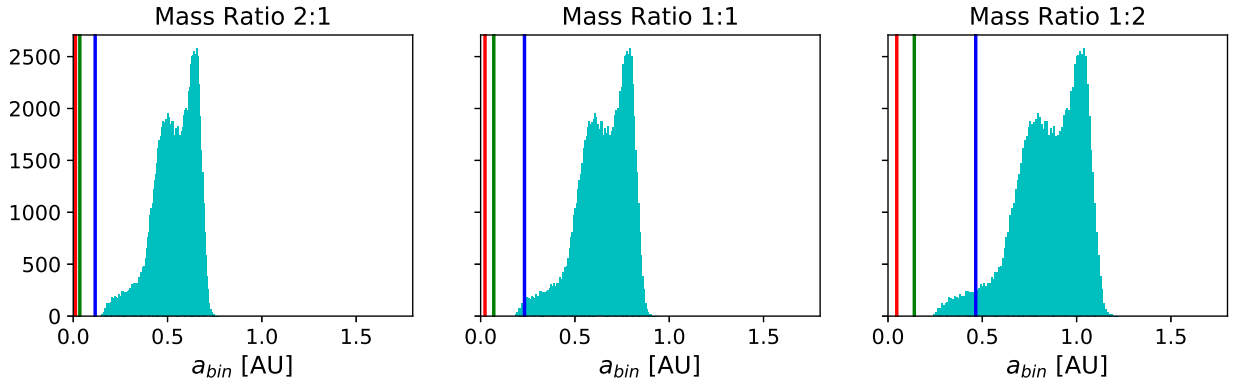

Figure D.10: HVS 13

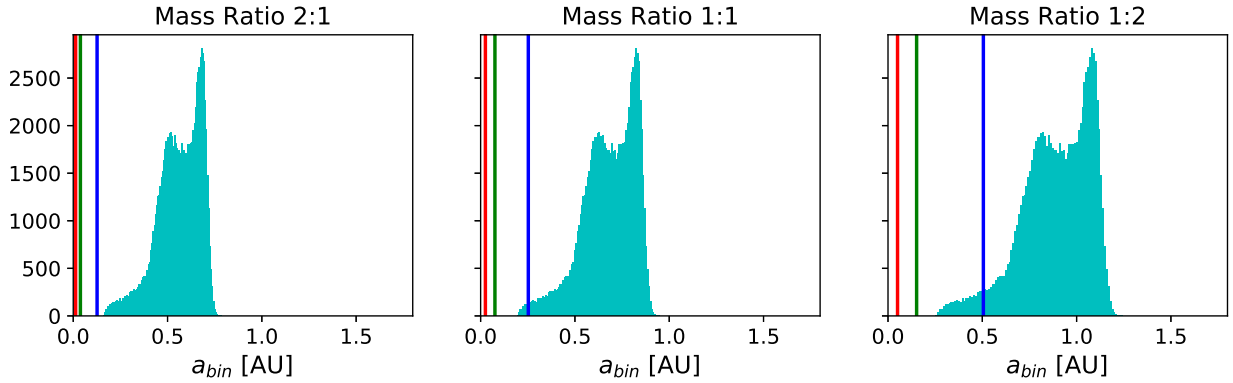

Figure D.11: HVS 14

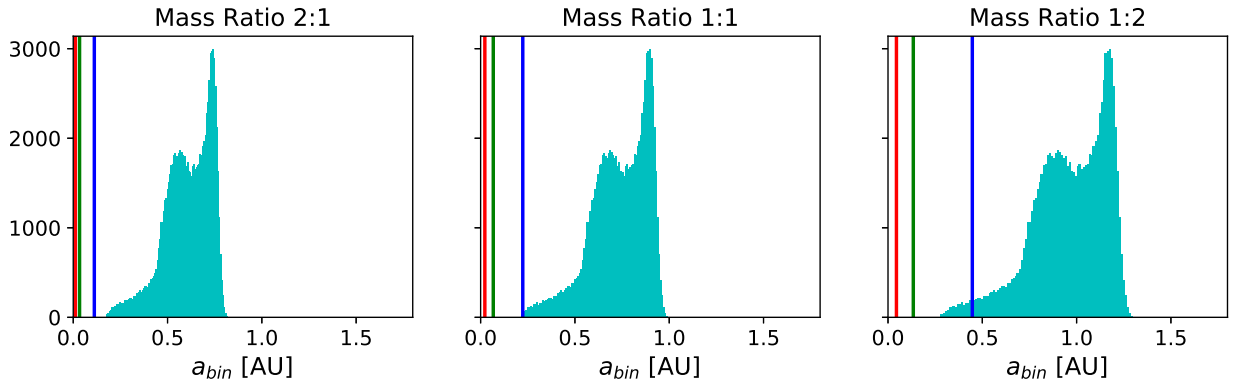

Figure D.12: HVS 15

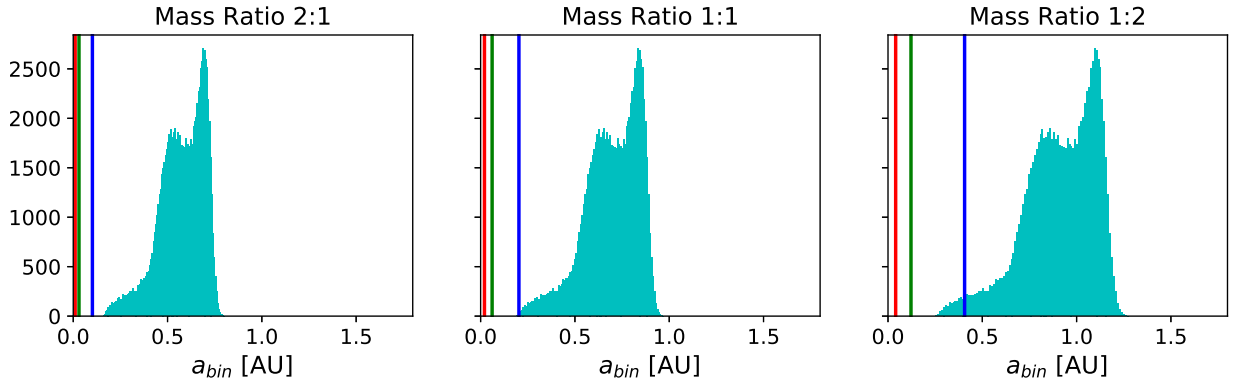

Figure D.13: HVS 16

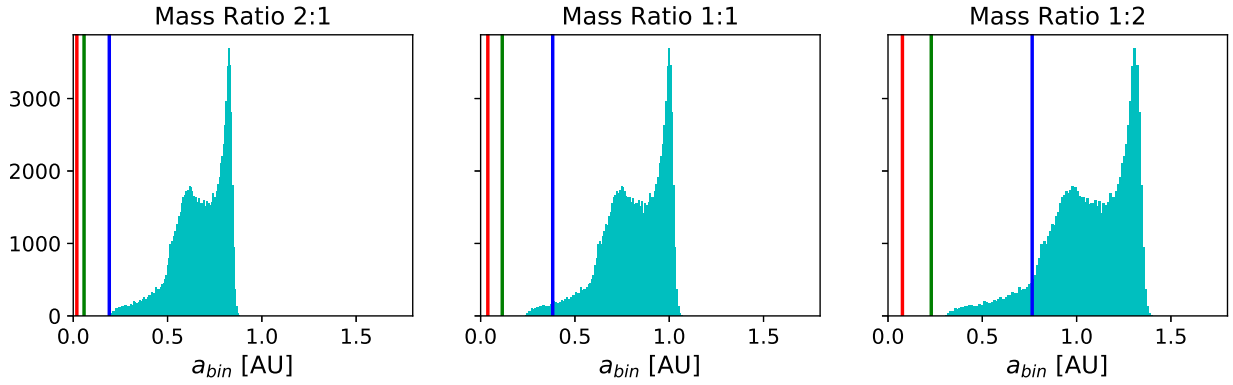

Figure D.14: HVS 17

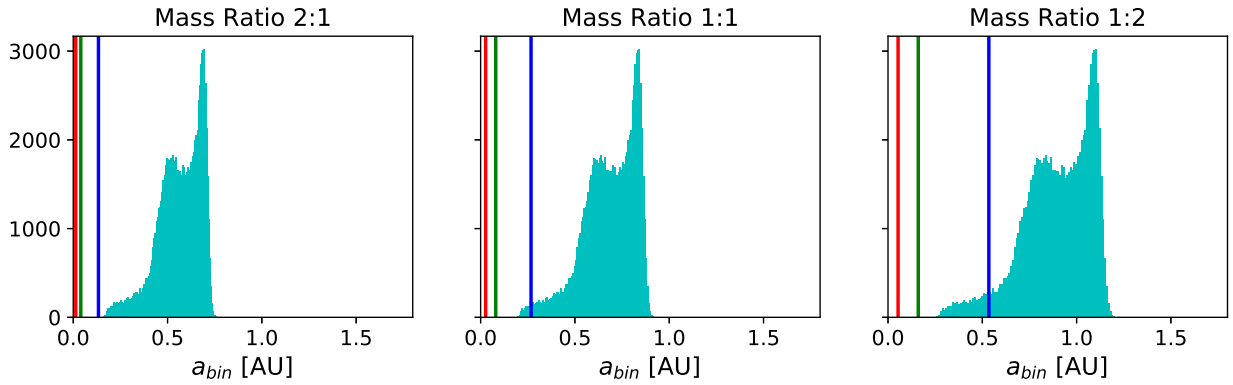

Figure D.15: HVS 18

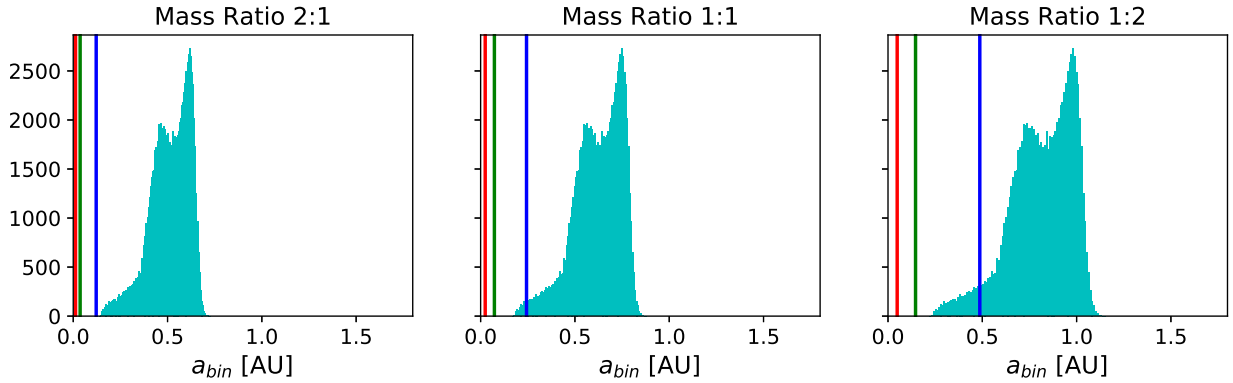

Figure D.16: HVS 19

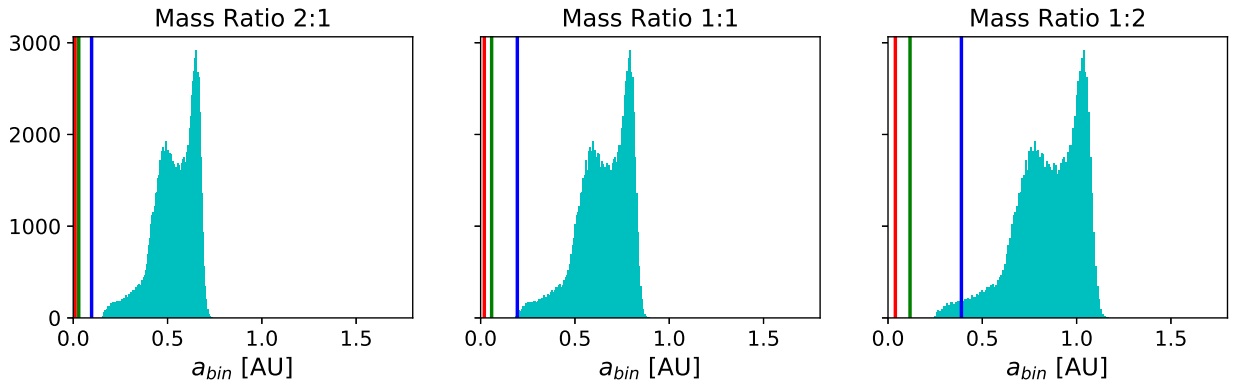

Figure D.17: HVS 20

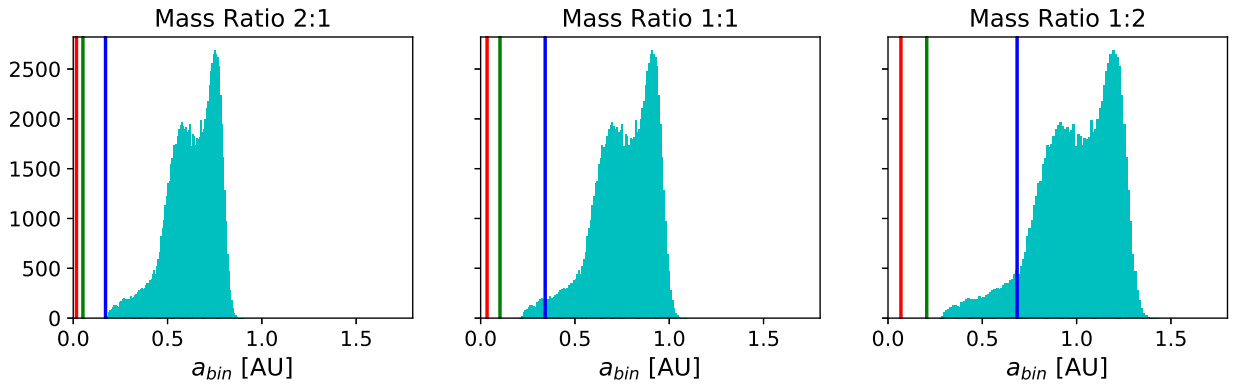

Figure D.18: HVS 21